Available online at www.sciencedirect.com
ScienceDirect
Geochimica et Cosmochimica Acta 70 (2006) 5293–5322
Geochimica
www.elsevier.com/locate/gca

A threshold in soil formation at Earth's arid–hyperarid transition

Stephanie A. Ewing [a,*], Brad Sutter [b], Justine Owen [a], Kunihiko Nishiizumi [c], Warren Sharp [d], Steven S. Cliff [e], Kevin Perry [f], William Dietrich [g], Christopher P. McKay [b], Ronald Amundson [a]

[a] *Division of Ecosystem Sciences, 137 Mulford Hall, University of California, Berkeley, CA 94720, USA*
[b] *NASA-Ames Research Center, Moffett Field, CA 94035, USA*
[c] *Space Sciences Laboratory, University of California, 7 Gauss Way, Berkeley, CA 94720, USA*
[d] *Berkeley Geochronology Center, 2455 Ridge Rd., Berkeley, CA 94709, USA*
[e] *Department of Applied Science, University of California, Davis, CA, USA*
[f] *Department of Meteorology, University of Utah, Salt Lake City, UT, USA*
[g] *Department of Earth and Planetary Science, McCone Hall, University of California, Berkeley, CA 94720, USA*

Received 25 January 2006; accepted in revised form 9 August 2006

Abstract

The soils of the Atacama Desert in northern Chile have long been known to contain large quantities of unusual salts, yet the processes that form these soils are not yet fully understood. We examined the morphology and geochemistry of soils on post-Miocene fans and stream terraces along a south-to-north (27° to 24° S) rainfall transect that spans the arid to hyperarid transition (21 to ~2 mm rain y^{-1}). Landform ages are $\geqslant$ 2 My based on cosmogenic radionuclide concentrations in surface boulders, and Ar isotopes in interbedded volcanic ash deposits near the driest site indicate a maximum age of 2.1 My. A chemical mass balance analysis that explicitly accounts for atmospheric additions was used to quantify net changes in mass and volume as a function of rainfall. In the arid (21 mm rain y^{-1}) soil, total mass loss to weathering of silicate alluvium and dust (-1030 kg m^{-2}) is offset by net addition of salts ($+170$ kg m^{-2}). The most hyperarid soil has accumulated 830 kg m^{-2} of atmospheric salts (including 260 kg sulfate m^{-2} and 90 kg chloride m^{-2}), resulting in unusually high volumetric expansion (120%) for a soil of this age. The composition of both airborne particles and atmospheric deposition in passive traps indicates that the geochemistry of the driest soil reflects accumulated atmospheric influxes coupled with limited in-soil chemical transformation and loss. Long-term rates of atmospheric solute addition were derived from the ion inventories in the driest soil, divided by the landform age, and compared to measured contemporary rates. With decreasing rainfall, the soil salt inventories increase, and the retained salts are both more soluble and present at shallower depths. All soils generally exhibit vertical variation in their chemistry, suggesting slow and stochastic downward water movement, and greater climate variability over the past 2 My than is reflected in recent (~100 y) rainfall averages. The geochemistry of these soils shows that the transition from arid to hyperarid rainfall levels marks a fundamental geochemical threshold: in wetter soils, the rate and character of chemical weathering results in net mass loss and associated volumetric collapse after 10^5 to 10^6 years, while continuous accumulation of atmospheric solutes in hyperarid soils over similar timescales results in dramatic volumetric expansion. The specific geochemistry of hyperarid soils is a function of atmospheric sources, and is expected to vary accordingly at other hyperarid sites. This work identifies key processes in hyperarid soil formation that are likely to be independent of location, and suggests that analogous processes may occur on Mars.

1. Introduction

The Atacama Desert is one of the driest locations on Earth, with soils that harbor ore-grade deposits of nitrate, iodate, and other rare salts (Ericksen, 1981). After more than a century of speculation about the origin of these

* Corresponding author. Fax: +1 510 643 5098.
E-mail address: saewing@nature.berkeley.edu (S.A. Ewing).

0016-7037/$ - see front matter © 2006 Elsevier Inc. All rights reserved.
doi:10.1016/j.gca.2006.08.020

deposits (Ericksen, 1981; Darwin, 1906; Böhlke et al., 1997; Pueyo et al., 1998; Michalski et al., 2004), recent stable isotope studies have shown that much of the nitrate and sulfate in these soils is derived from atmospheric sources (Böhlke et al., 1997; Rech et al., 2003; Bao et al., 2004; Michalski et al., 2004). However, little is known about the post-depositional processing of atmospheric inputs within these soils, or the effect of climate on their geographical distribution (Berger and Cooke, 1997; Rech et al., 2003; Bao et al., 2004). Because of their unusual salt content, the soils of the Atacama Desert are sometimes portrayed as bizarre phenomena within an equally unusual climate regime. Here, we show that soil formation in this region simply reflects a critical shift in the balance of pedogenic processes as a function of extreme aridity.

Soil formation is a mass balance between inputs and losses, integrated over geological timescales (Brimhall et al., 1992; Amundson, 2004). Inputs to the starting parent rock or sediment are water, organic matter, and atmospheric salts and dust. Dissolved losses result from chemical weathering and transport of solutes out of the surficial weathering zone. On level and geomorphologically stable landforms in humid regions, the long-term ($\geqslant 10^5$ y) trajectory of soil development is a net mass loss and volumetric collapse via chemical weathering (Brimhall et al., 1992; Chadwick and Goldstein, 2004), because dissolved losses outpace the on-going addition of dust and solutes (e.g., Chadwick et al., 1999; Kurtz et al., 2000). With decreasing precipitation, dissolved losses are reduced (Chadwick and Goldstein, 2004). In arid settings, the slow accumulation of atmospheric inputs may lead to net mass gains of salts such as $CaCO_3$, as well as silicate dust (e.g., McFadden et al., 1987; Quade et al., 1995; Capo and Chadwick, 1999).

The low rainfall levels in the Atacama Desert represent the most arid extreme of a systematic decline in rainfall with decreasing latitude (i.e., south to north) in northern Chile. The duration of this climate pattern remains subject to debate, but geological (Hartley and Chong, 2002) and marine (Ravelo et al., 2004) records suggest it has existed since the late Pliocene. As a result, soils along this latitudinal gradient represent a long-term natural experiment revealing the geochemical effects of the transition from low to negligible rainfall. In this study, we combined measurements of the rate and composition of atmospheric deposition with total soil chemical analyses and landform age determinations, to assess net geochemical and volumetric change as a function of arid to hyperarid rainfall levels (21 to $\sim$2 m y^{-1}). This natural gradient provides insights into processes controlling the geochemistry of soils at the arid extreme on Earth, and the analog they provide for other hyperarid settings on Earth and Mars.

1.1. Geomorphology and climate

The Atacama Desert is located between about 17° and 27 °S latitude in northern Chile, bounded on the east by the front ranges of the Andes (Precordillera) and on the west by the Coast Range. In this intermontane zone (locally called the Central Depression), late Cenozoic fluvial sediment surrounds small, rounded to angular mountains (1500–3000 masl). South of about 23°S, the Atacama Desert is dominated by extensive, gravelly fluvial deposits, generally referred to as the Atacama Gravels (Mortimer, 1973; Naranjo and Puig, 1984; Godoy and Lara, 1998; Lara and Godoy, 1998). The Atacama Gravels and related deposits are thought to have resulted from uplift of the Andes, terminating in middle to late Miocene time (Clark et al., 1967; Mortimer, 1973; Marinovic et al., 1992; Nishiizumi et al., 2005). Subsequent incision into the Atacama Gravels resulted in prominent and extensive, late Miocene to Pliocene age fans and terraces (Mortimer, 1980; Godoy and Lara, 1998; Lara and Godoy, 1998; Hartley et al., 2005 also see discussion below for age controls). These landforms host well-developed soils rich in nitrate and other salts, and are the focus of this study.

Temperature and precipitation vary with both latitude and elevation within the Atacama Desert. Mean annual temperatures (MAT) range between 10 and 16 °C (mainly varying with elevation and proximity to the coast). Mean annual rainfall (MAR) based on rain gage data in the region (1000–2000 m above sea level, 17–27 °S) is less than 50 mm, generally falling in austral winter and decreasing with latitude in the coastal desert (Houston and Hartley, 2003; Vuille and Keimig, 2004). Marine fog is frequent along the coast at these latitudes (Schemenauer and Cereceda, 1992; Larrain et al., 2002), but inland incursion of this fog, as well as formation of inland radiation fogs, depends on elevation and topographic connection to the coast (Cereceda et al., 2002). Potential evapotranspiration (PET) is $\sim$1–2 mm d^{-1} (Mintz and Walker, 1992), making rainfall levels below 20–40 mm y^{-1} "hyperarid" (MAP/PET < 0.05; UNEP, 1991). In this study, estimates of MAT and MAR are based on ongoing monitoring at our selected sites and from other local rain gauge data over the last century (see below; McKay et al., 2003; Warren-Rhodes et al., 2006). Generally as rainfall levels drop with decreasing latitude, rainfall events are less frequent. In the most hyperarid zone, a decade may pass without rain, followed by a single rainfall event of 10–20 mm (Warren-Rhodes et al., 2006).

Several factors contribute to the longer-term aridity of the Atacama Desert (Houston and Hartley, 2003; Hartley et al., 2005). Global atmospheric circulation generates a zone of high pressure just offshore, blocking westerly moisture sources, and uplift of the Andes has produced a rain-shadow effect, combining with continentality to block easterly rainfall sources. Upwelling cold water along the Atacama coast helps to prevent rain derived from the nearby Pacific. These factors have been used in support of geological evidence that the Atacama Desert has been hyperarid for 9 to 15 My or more (Alpers and Brimhall, 1988; Clark et al., 1990; Hartley et al., 2005; Hartley and Rice, 2005). However, estimates of the duration of continuous hyperaridity vary greatly, from 2 to 4 My based on

stratigraphic evidence (Hartley and Chong, 2002; Houston and Hartley, 2003; Hartley et al., 2005) to ~25 My based on CRN-derived landform exposure times (Dunai et al., 2005). On shorter timescales, rainfall oscillations have occurred in areas immediately peripheral to the Atacama's hyperarid core, a region of persistent "absolute desert" (Betancourt et al., 2000; Lamy et al., 2000; Latorre et al., 2002; Latorre et al., 2003). In general, a hyperarid climate, subject to shorter term rainfall oscillations, has characterized the Quaternary history of the region.

Throughout our field area, the presence of extensive fluvial landforms of approximately late Pliocene age, and the relatively limited extent of clearly Quaternary features, suggests a profound Plio-Pleistocene aridification, consistent with other work (Hartley and Chong, 2002; Ravelo et al., 2004; Hartley et al., 2005). Therefore, we focused on the geochemistry of mature landforms likely to be Pliocene in age. The soils developed on these landforms should integrate shorter-term rainfall oscillations, and reveal the long term (10^6 y) effects of the latitudinal rainfall gradient.

1.2. Nitrate deposits, soils and vegetation

The nitrate-rich deposits of northern Chile have been the most studied aspect of Atacama Desert geochemistry (e.g., Ericksen, 1981; Pueyo et al., 1998; Searl and Rankin, 1993). These deposits are a subset of Atacama soils in which nitrate is concentrated into commercially viable quantities (>5% by mass) by several processes (Ericksen, 1981; Pueyo et al., 1998; Searl and Rankin, 1993). In general, nitrate-rich soils mantle the landscape, with highest concentrations found adjacent to, or downwind of, playas or salars. Despite interest in the nitrate deposits, preliminary studies of Atacama soils have not fully characterized their geographical distribution (Mikhailov, 2000) although east–west variation in soil chemistry, due to increasing distance from marine sources of atmospheric particles, has been demonstrated (Berger and Cooke, 1997; Rech et al., 2003). In this study, we minimized this variation by selecting sites roughly equidistant from the coast.

Plant communities in the Atacama Desert are indicators of water availability via rainfall and/or fog, and follow pronounced latitudinal and elevational climatic gradients (e.g., Latorre et al., 2003). In the hyperarid core, rainfall is currently insufficient to support vascular plants except in isolated washes (Latorre et al., 2002; Latorre et al., 2003), and primary production is principally limited to slow-growing cyanobacteria that survive under select translucent stones (e.g., quartz; Warren-Rhodes et al., 2006) and within some precipitated salts (e.g., gypsum and halite; Dong et al., 2006; Wierzchos et al., 2006). This "absolute desert" is bounded by coastal lomas (areas of highly fog-adapted plants) in the Coast Range to the west and prepuna vegetation in the Precordillera to the east (>2700 m) (Latorre et al., 2002, 2003). To the south of about 26 °S, there is a transition from plants that are confined to dry washes and other locations where water availability is increased (including hillsides that intercept fog), to more continuous vegetation, as a function of more frequent winter rain from Pacific westerlies (Latorre et al., 2002). In this study, we examine soils spanning the transition from sparse but continuous vegetation with arid conditions to the south, to the total absence of plants in the hyperarid core of the northern desert.

1.3. Atmospheric deposition

Taken together, previous work on soils and nitrate ores in the Atacama Desert points to the potential importance of two categories of atmospheric sources of soil materials: (1) eolian redistribution of particles (dust, sea-salt, salar salts) and (2) particles formed locally by atmospheric chemistry (e.g., nitrate and sulfate compounds from gaseous oxide precursors; Michalski et al., 2004). Marine upwelling immediately offshore leads to high biological productivity in the coastal ocean (Marín and Olivares, 1999; Moore et al., 2002). As a result, marine aerosols in this area are a likely source of not only primary sea salt constituents (e.g., Na and Cl) but also of inorganic S (Rech et al., 2003) and N (Michalski et al., 2004) in soils. Marine biological sources may also supply organic C and N, as well as Ca and inorganic C from marine organisms (Moore et al., 2002). The relatively continuous inputs of sea salt with pervasive onshore winds may be supplemented by volcanic emissions from the east, though these sources are poorly quantified and likely to be highly variable (Matthews et al., 1997; Mather et al., 2004a,b). Volcanic or groundwater-derived salts are also dispersed through the region by eolian deflation of salars (playas) (Spiro and Eckardt, 1999; Rech et al., 2003; Bao et al., 2004; Bao, 2005). Ultimately, local soil chemistry is likely to be spatially variable, and will depend on proximity to atmospheric sources (Rech et al., 2003). In this study, we chose sites either upwind or physically removed from salars or other obvious terrestrial dust sources, and at a similar distance from the coast. These sites should reflect the regional influx and deposition of atmospheric particles, with a relatively consistent marine component among sites.

2. Methods

2.1. Site characteristics and soil sampling

We selected three sites on stable, ancient landforms along a south–north transect (Fig. 1). These sites follow the transition from soils supporting continuous plant cover (arid) to those with a complete absence of vegetation (hyperarid). Sites were chosen to minimize differences in factors other than MAR. All sites are located at similar elevations and distances from the coast, and should be subject to similar fog frequency and marine influences. Parent material is dominantly local Mesozoic granitic alluvium (Naranjo and Puig, 1984; Marinovic et al., 1992; Arévalo, 1995). The landforms we selected are mapped as Quaternary

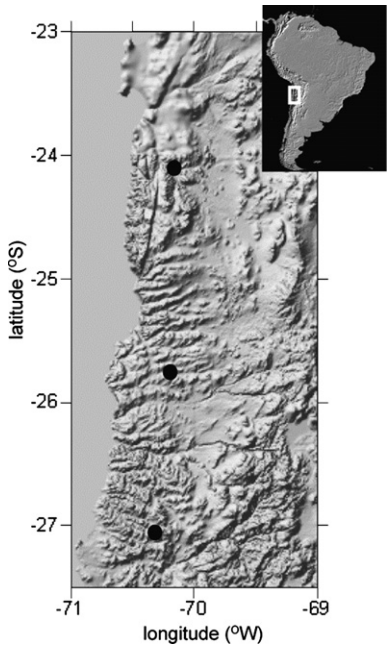

Fig. 1. Site locations in study. From north to south are Yungay (<2 mm rain y^{-1}), Altamira (~10 mm rain y^{-1}), and Copiapó (~20 mm rain y^{-1}).

to Pliocene in age (Naranjo and Puig, 1984; Marinovic et al., 1992; Arévalo, 1995). Using these maps as a starting guide, our field selection strategy was to choose landforms that are areally extensive, stratigraphically higher than local Quaternary washes, and stratigraphically lower than the prominent regional Miocene gravels. The most recent regional geologic mapping supports the hypothesis that these landforms are Pliocene in age (Naranjo and Puig, 1984; Marinovic et al., 1992; Arévalo, 1995; Godoy and Lara, 1998; Lara and Godoy, 1998), and we tested this hypothesis with landform age measurements using cosmogenic radionuclide concentrations in surface boulders, and Ar isotope dating of interbedded ash layers near the driest site (see Section 2.2). Depending on location, our selected sites are either alluvial fan surfaces (Yungay, Copiapó) or stream terraces (Altamira). The final soil locations were based on numerous preliminary excavations in the area, and on observations of road cuts and mining excavations. We attempted to select sites distinct enough that the overall effects of MAR on soil characteristics exceeded this local variability.

Continuous monitoring since 2001 or earlier (McKay et al., 2003), and local records (both coastal towns and select inland sites) dating to the turn of the century, indicate that mean annual precipitation decreases from 21 to $\leqslant$2 mm y^{-1} between the southern (Copiapó) and northern (Yungay) sites, respectively (Houston and Hartley, 2003; Warren-Rhodes et al., 2006). With PET of ~400 mm y^{-1} at these sites (Mintz and Walker, 1992), this indicates that the Copiapó site is transitional between "arid" and "hyperarid" (MAP/PET ~ 0.05; UNEP, 1991). Evidence of rainfall fluctuations (e.g., Latorre et al., 2002) indicates that these MAP averages are likely lower than the longer term (10^6 y) averages relevant to these soils, but it is likely that the north–south MAP gradient has persisted through time (Mortimer, 1980; Hartley et al., 2005).

Soil pits were excavated in 2001 and 2002 at each site to ~2 m, by hand and with a jackhammer. The salt-indurated horizons found in all soils made hand excavation to fresh sediment impractical or impossible. Even with a jackhammer, we were unable to fully penetrate the sulfate cemented zone at Altamira. Soils were described using standard methods (NSSC, 2002), and were sampled by identified horizons. Field descriptions included qualitative tests for carbonate effervescence with 1 M HCl; nitrate was assayed using a field analyzer (Spectrum Technologies, Inc.). Bulk density of each horizon (including gravel) was measured using a combination of three techniques: (1) collection of core samples of known volume, (2) field measurement of the mass of an excavated volume of soil, and/or (3) collection of intact peds in paraffin or saran and determination of their volume by displacement of water.

2.2. Landform age determination

While geologic mapping provides a starting guide for soil age (Naranjo and Puig, 1984; Marinovic et al., 1992; Arévalo, 1995; Godoy and Lara, 1998; Lara and Godoy, 1998), we conducted geochronological studies to more accurately constrain the time of soil formation. We determined surface boulder exposure ages using in situ cosmogenic ^{10}Be and ^{26}Al concentrations (Kohl and Nishiizumi, 1992) in quartz grains from boulders located on the land surface. Three boulders of granitic composition ranging from approximately 30 to 60 cm in diameter were selected at each site. We hypothesized that the boulders had been exposed continuously since deposition because the surface pavement at all sites (including boulders) rests on a mantle of atmospherically derived salts and dust (e.g., McFadden et al., 1987) that is nearly devoid of coarse fragments and has likely accumulated continuously over time (see discussion below). Using a jackhammer, the outermost 1–2 cm of the tops of the boulders was removed for subsequent processing. Age calculations include correction for boulder orientation. Care was taken to choose boulders with limited evidence of wind erosion.

Approximately 500 g of rock was ground, and quartz grains were isolated through a series of acid treatments (Kohl and Nishiizumi, 1992). ^{10}Be and ^{26}Al were isolated and purified using anion and cation exchange columns. Accelerator mass spectrometer (AMS) measurements of ^{10}Be and ^{26}Al were performed at the Lawrence Livermore National Laboratory AMS facility. The results were converted to minimum exposure ages and maximum erosion rates using the production rate scaling factors of Lal (1991) and site-specific location data. Although we collected samples from three boulders on each terrace, processing problems left us with only one sample for Yungay and Copiapó, and two samples from Altamira (Altamira-1

and Altamira-3). To explore the exposure times at Altamira further, ^{21}Ne, a stable cosmogenic isotope, was also measured in quartz from the boulder Altamira-1. This analysis was performed at the Institute of Geology, ETH Zurich by Florian Kober and Rainer Wieler.

An upper limit on the age of the alluvial fan containing the Yungay site is provided by ^{40}Ar/^{39}Ar dating of sanidines from ash layers in a nearby, correlative fan deposit. Ash samples Yungay-02-UL and Yungay-02-L were collected from two water-laid, silicic ash layers interbedded with alluvium approximately 0.25 and 1.5 m, respectively, below the surface of a fan mapped as part of the same geological unit as the Yungay fan (Marinovic et al., 1992). Single-crystal, laser-fusion analyses of eleven to fifteen >300 μm sanidine grains from each of these samples were carried out at the Berkeley Geochronology Center using techniques similar to Deino and Potts (1990). Neutron irradiation procedures and corrections for interfering argon isotopes follow those of Renne et al. (1998).

2.3. Composition and rates of atmospheric deposition

Atmospheric deposition was measured using passive collectors (Reheis and Kihl, 1995) at the three soil sites. These collectors, or traps, consist of a layer of acid-washed glass marbles suspended in a 310 cm^2 pan, elevated ~1.5 m off the ground on poles to avoid accumulation of saltating sand. Multiple pans were deployed near each site and collected after ~1 y in 2002 and 2004. Marbles were transferred to a 3-L HDPE bottle and covered with about 750 mL distilled-deionized water. Pans were rinsed into 250-mL HDPE bottles with about 200 mL distilled-deionized water. All bottles were shaken for 1 h to dissolve water-soluble salts. Each suspension was then filtered through a 0.45 μm nylon filter, and the resulting solution was analyzed for soluble components using ion chromatography (IC) and inductively coupled plasma—atomic emission spectroscopy (ICP-AES). The solid portion of the dust was analyzed for major elements by inductively coupled plasma-mass spectrometry (ICP-MS) and ICP-AES. XRD was performed on the clay fraction (<2 μm) of dust samples from the Yungay and Copiapó sites.

Air samples were also collected using two active sampling methods: (1) filtration: air was pumped through a filter at a known rate, with or without a size-limiting jet; and (2) impaction: air was directed through a series of sized openings and impaction plates at a known rate, allowing particles to impact onto Teflon filters according to their diameter. All sampling units were battery operated and mounted on 2 m ladders. Batteries were changed every 24 h, for a total collection time of about 72 h. Three replicate sample sets were collected at each site. In October 2002, we collected total suspended particles on 47 mm Teflon filters using Mini-Vol pumps (Airmetrics Inc.; 5 L min^{-1}) near each of the three soil sites. These samples were analyzed by X-ray fluorescence (XRF) for total chemistry, and by IC (anions), autocolorimetry (ammonium), and atomic absorption (soluble metals) for water-soluble chemistry, at the Desert Research Institute in Reno, Nevada. In January 2004 at Altamira and a coastal site, we collected airborne particles by size using small cascade impactors (SKC, Inc.), PM10 inlets (SKC, Inc.) and battery-operated pumps (BGI, Inc.; 9.0 L min^{-1}) to collect airborne particles in four size fractions (<0.5, 0.5–2.5, >2.5, <10 μm) on Teflon filters. The 2004 samples were analyzed by synchrotron-XRF at the Advanced Light Source, Lawrence Berkeley National Laboratory, beamline 10.3.1 (Perry et al., 2004).

2.4. Soil chemistry

Soil samples were sieved to obtain a <2 mm fraction for subsequent analyses, in order to reduce error due to variable gravel content. Care was taken to break up encrusted salts, so that only silicate rock fragments >2 mm (“gravel”) were excluded. Gravel concentrations were accounted for in subsequent calculations of total elemental inventories and strain (see below).

Nitrate and ammonium were determined in aqueous extracts (20:1 (water/soil or 2 M KCl/soil) by mass) using a Lachat autoanalyzer (Lachat Instruments, Milwaukee, WI). Sulfate, nitrate and chloride concentrations in these same extracts were also determined by IC for select samples (Dionex). Water soluble Ca^{2+}, Mg^{2+}, Na^{+}, and K^{+} were determined by ICP-AES (Thermo Jarrel Ash HR). Due to high concentrations and limited solubility of gypsum and anhydrite, we report total Ca and S results as water-soluble concentrations in horizons where these elements occur at very high levels (>500 μmol g^{-1}). Three replicate extracts were analyzed for each horizon, along with a sample blank.

Total chemistry for major elements was determined using ICP-MS and ICP-AES on a lithium–borate fusion of each soil sample. Total S analysis was by Leco furnace and infrared spectroscopy. Inorganic C (carbonate) was determined by HCl leach and Leco-gasometric finish. To identify mineralogy in the fine soil fraction (<2 mm), X-ray diffraction (XRD) was performed on whole samples and on the clay fraction (size cuts 2–0.2 and 0.2–0.08 μm) from horizons at 1, 33 and 186 cm depth in the Yungay soil. XRD treatments included Mg-saturation, Mg-saturation with glycol, K-saturation, and K-saturation plus heating (550 K). The removal of salts and particle size separation followed the procedure of Whittig and Allardice (1986). Glycol was used in place of glycerol for detection of expanding clays.

Organic C was determined by sealed tube combustion (Minagawa et al., 1984) of ~1 g of soil following (1) a distilled, deionized water rinse of select samples to remove halite and gypsum/anhydrite; and (2) addition of 1 M 100% phosphoric acid to remove carbonate, followed by freeze drying rather than rinsing (to prevent acid hydrolysis and loss of OC). The liberated carbon dioxide was cryogenically purified, and its quantity was determined manometrically.

2.5. Mass balance model for arid to hyperarid soils

The Atacama Desert is a unique environment because atmospheric inputs (silicate dust and salts) have accumulated in soils over time with small to negligible weathering losses. Because we have selected sites on ancient alluvial landforms that have been subject to minimal erosion, we hypothesized that dissolution and downward transport are the primary means of mass loss in these soils—a loss that decreases with increased hyperaridity. Decreased dissolved losses and increased retention of atmospheric inputs makes the mass balance of hyperarid soils fundamentally different from that of soils in wetter climates. In this section, we present a conceptual model for soil mass balance behavior as MAR declines to very low levels. These hypotheses then guide our subsequent interpretation of the chemical data with rainfall.

We used a soil mass balance that accounts for both chemical and volumetric changes of soil relative to its "parent material"—the rock or sediment from which the soil formed (Brimhall et al., 1992). This approach requires selection of two critical chemical parameters: (a) a reference "parent material", and (b) an "immobile" index element that has been quantitatively retained during soil formation. However, the addition of silicate dust that contains the "immobile" element complicates the mass balance (e.g., Brimhall et al., 1992), and is not always explicitly dealt with in geochemical studies. Given the clear accumulation of atmospheric salts in these soils, atmospheric inputs are considered non-trivial in this study.

Fig. 2 illustrates soil mass balance effects as rainfall varies in ancient soils. If physical erosion is negligible, a general soil mass balance statement that accounts for addition of silicate dust and salts is:

$$m_w = m_p + m_b + m_d + m_s - m_l \quad (1)$$

where m_w is the mass of the weathered substrate (soil), m_p is the original mass of the in situ parent material, m_b is the mass of material added through biological activity, m_d is the mass of the added silicate dust, m_s is the mass of the added salts, and m_l is the mass of dissolved losses due to chemical alteration or simple dissolution (Fig. 2).

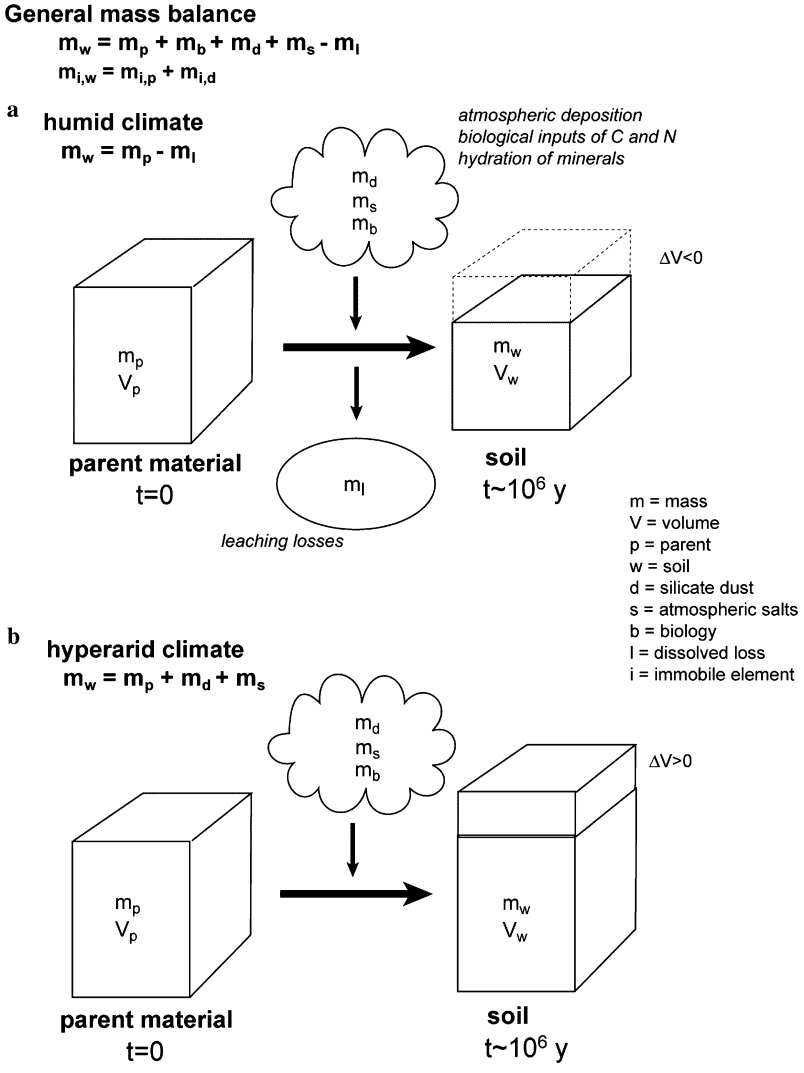

Fig. 2. Soil mass balance parameters.

This mass balance represents a single point in time. Soil formation is reflected in the difference in mass between the soil at that time and the geologic material (in this case, alluvium) from which the soil formed. Total mass gain or loss (Δ_m) during soil formation has been defined (Brimhall et al., 1992) as the mass difference between the mass of the "proto-ore" or parent geologic substrate (m_p) and the corresponding mass of the weathered substrate (m_w):

$$\Delta_m = m_w - m_p \quad (2a)$$

As further discussed below, addition of silicate dust that geochemically resembles the parent geologic substrate complicates the mass balance. In this study, we focus on solute addition and therefore consider both the starting alluvium (soil gravels) and the added silicate dust (non-water soluble material in deposition traps) as "parent material" ($m_{p+d} = m_p + m_d$). The mass change then becomes

$$\Delta_m = m_w - m_{p+d} \quad (2b)$$

Similarly, for any mobile element (j)

$$\Delta_j = m_{j,w} - m_{j,p+d} \quad (2c)$$

In humid climates ($\geqslant 10^3$ mm rain y^{-1}) over long time periods (10^5–10^6 y), weathering losses far exceed atmospheric and biological inputs (Fig. 2a). Atmospheric inputs may contribute only the less soluble species to the net mass balance, and soluble components such as nitrate and sulfate are not retained at all (Kurtz et al., 2001). Therefore, the long-term mass balance is primarily a function of net losses from parent material ($m_w \approx m_p - m_l$), and soil formation is a process of mass loss ($\Delta_m = -m_l$).

In arid soils (10^1–10^2 mm rain y^{-1}), atmospheric inputs may partially balance dissolved losses. The Copiapó site falls within this climate category. A small portion of atmospherically derived salts such as sulfate may be retained, and silicate dust may also accumulate, but limited dissolved loss of elements such as Si may also occur. Because these soils lie at the climate "hinge" or threshold between net gains or losses, a small increase in rainfall may tip the balance toward net chemical weathering losses. Soils that exhibit both small gains of soluble atmospheric solutes and small losses of rock-derived elements (two generally incompatible processes) likely reflect variable climate conditions over time.

For an arid soil that has been subject to losses (m_l) and salt addition (m_s) but has minimal biological inputs, the mass change relative to parent alluvium plus dust is:

$$\Delta_m = m_s - m_l \quad (2d)$$

At the hyperarid extreme ($<10^1$ mm rain y^{-1}; Fig. 2b), all atmospheric inputs are retained, and dissolved losses and biological activity are negligible ($m_w \approx m_p + m_d + m_s$). Here, the driest site (Yungay) represents this climate category. In this case, soil formation occurs by mass addition. The total mass gain relative to parent alluvium plus dust is equal to the total mass of salts:

$$\Delta_m = m_s \quad (2e)$$

2.5.1. Soil mass balance calculations

A summary of the symbols used in this section is included in Table 1.

The relative change in the total mass of material with weathering can be determined from the concentration an immobile element (i) in the parent geologic substrate (p) and the weathered substrate (w). An element is truly immobile if it is neither added to nor lost from the mass of parent material during weathering. The mass of an immobile element in the parent material ($m_{i,p}$) will be identical to the mass in the weathered soil ($m_{i,w}$)

$$m_{i,w} = m_{i,p} \quad (3a)$$

If an element is immobile against weathering, but is added with silicate dust (d), then

$$m_{i,w} = m_{i,p} + m_{i,d} \quad (3b)$$

Commonly used immobile elements are Zr, Ti and Nb. In this paper we use Zr, and make the simplifying assumption that the concentration of the immobile element in silicate dust added to these soils over time is equal to the concentration in the parent alluvium in which these soils developed ($C_{i,d} = C_{i,p} = C_{i,p+d}$). This assumption is generally supported by our analysis of immobile element concentrations in silicate dust, gravels from soil horizons and local washes, and wash fines (Table 2). With this assumption, the change in total soil mass relative to the mass of parent alluvium plus dust (T; equivalent to the "chemical depletion fraction" of Riebe et al., 2001) can be determined from the ratio of immobile element concentrations

Table 1
Symbols

Symbol	Definition
T	Change in total soil mass vs. parent mass (kg kg^{-1})
M	Change in total soil mass vs. area (kg m^{-2})
$\overline{M}$	Depth-integrated value of M
ε	Change in total soil volume vs. parent volume (m^3 m^{-3})
$\tau_{j,w}$	Change in amount (g or mol) of element j per mass of j in parent (alluvium plus dust) (kg kg^{-1})
α_j	Change in amount (g or mol) of element j per mass soil (kg kg^{-1})
M_j	Change in amount (g or mol) of element j per area (kg m^{-2})
Ca_{Zr}	α_{Ca} using Zr as the immobile element

Table 2
Reference ("immobile") elements in candidate parent materials

Site	Reference[a]	Soil gravel	Insol. dust	Wash gravel	Wash fines
Yungay	TiO_2 (%)	0.41–0.66	0.59	0.66	0.53
Altamira	TiO_2 (%)	0.33–0.55	0.74	0.71	0.82
Copiapó	TiO_2 (%)	0.67–1.03	0.59	1.16	1.39
Yungay	Zr (ppm)	160–186	123	194	186
Altamira	Zr (ppm)	119–169	102	172	145
Copiapó	Zr (ppm)	80–243	122	148	207
Yungay	Nb (ppm)	7.0–7.3	8	8	8
Altamira	Nb (ppm)	6–9	6	7.5	9.5
Copiapó	Nb (ppm)	8–10	7	11	15

[a] Observed variabilities are 0.20% for TiO_2, 20 ppm for Zr, and 1 ppm for Nb.

$$T = \frac{\Delta_m}{m_p + m_d} = \frac{C_{i,p+d}}{C_{i,w}} - 1 \quad (4)$$

This is analogous to considering the combined silicate dust and parent alluvium as "parent material," though clearly they are acted upon by in situ soil chemical weathering for differing time periods. With this approach, the relative mass of added dust (m_d) vs. starting alluvium (m_p) does not affect these mass change calculations. However, it does become important for volume change (see below).

The total mass change on an area basis (M) is

$$M = \frac{\Delta_m}{A} = \frac{\rho_w h_w (C_{i,p+d} - C_{i,w})}{C_{i,p+d}} \quad (5)$$

where A is area of the land surface, ρ is bulk density (e.g., g cm^{-3}) and h is depth (e.g., cm). At arid sites that exhibit both salt additions and dissolved losses (Eq. (2d)), salts can be measured independently and subtracted (as mass per area) from the depth-integrated, apparent mass loss ($\overline{M}$) to estimate the total mass loss to silicate transformation. At the hyperarid extreme (Eq. (2e)), the total, depth-integrated mass change ($\overline{M}$) relative to parent alluvium plus silicate dust should equal the depth-integrated, directly measured salt inventory. These two measures of salt addition can be compared in order to test the validity of the assumption that $C_{i,p} = C_{i,d}$. The mass of salts at the hyperarid extreme should represent total salt deposition to all sites, and can be used to estimate salt losses at wetter sites.

For elemental mass changes, a useful way to account for the effect of starting concentration in parent material is to compare mass change in mobile element j relative to the mass of j originally present in the parent material (τ_j; Brimhall et al., 1992; Amundson, 2004). If $C_{i,p} \approx C_{i,d}$ and $C_{j,p} \approx C_{j,d}$, the elemental mass change relative to the amount of that element in parent alluvium plus dust is

$$\tau_{j,w} = \frac{\Delta_j}{m_{j,p} + m_{j,d}} = \frac{C_{j,w} C_{i,p+d}}{C_{j,p+d} C_{i,w}} - 1 \quad (6)$$

Because τ values are defined relative to the amount of the element of interest in parent material, they normalize results for the effects of variable starting concentrations in parent material. However, τ values are undefined for the case where $C_{j,p} = 0$ and are uninformative for elements where additions over time far exceed what was present in parent material ($\tau \gg 1$). Exceedingly large τ values occur primarily for biologically concentrated elements such as C or N, or in hyperarid environments for elements such as S and Cl that are added in large amounts by atmospheric deposition over long times. Under these circumstances, mass gains and losses may also be most effectively considered relative to the mass of soil (m_w) to give them units of concentration in soil (μg g^{-1} soil):

$$\alpha_{j,w} = \frac{\Delta_j}{m_w} = C_{j,w} - C_{j,p+d} \frac{C_{i,w}}{C_{i,p+d}} \quad (7)$$

Positive values of $\alpha_{j,w}$ represent the portion of element j in the soil mass that was not present in the parent material. If additions of an element are large relative to the starting amount in the parent material ($\tau_j \gg 1$), or if an element was not present in parent material, net mass additions relative to soil mass will simply equal soil concentration values ($\Delta_j \approx m_{j,w}$; $\alpha_{j,w} \approx C_{j,w}$). If an element has been added with salts but has also been lost to a lesser degree in chemical transformation of parent material, $\alpha_{j,w} < C_{j,w}$. With constant net inputs and losses (and inputs > losses), α will increase linearly with time.

Finally, the total elemental mass change on an area basis, relative to parent alluvium plus dust is

$$M_j = \frac{\Delta_j}{A} = \rho_w h_w \left[C_{j,w} - \frac{C_{j,p+d} C_{i,w}}{C_{i,p+d}} \right] \quad (8)$$

2.5.2. Volumetric strain

Mass gain or loss typically is associated with volumetric change, which has been termed "strain" (Brimhall and Dietrich, 1987). Notably, a simple change in pore space (e.g., increase via bioturbation or decrease by compaction) will change volume without changing mass. The total volumetric change (expansion or collapse) of soil (w) relative to starting parent material (p) can be determined by using immobile element concentrations to normalize the ratio of bulk densities (Brimhall and Dietrich, 1987; Brimhall et al., 1992):

$$\varepsilon_{i,w} = \frac{\Delta_v}{V_p} = \frac{V_w - V_p}{V_p} = \frac{V_w}{V_p} - 1 = \frac{\rho_p C_{i,p}}{\rho_w C_{i,w}} - 1 \quad (9a)$$

where V is volume. In salt-indurated Atacama Desert soils, the underlying fluvial sediment was physically difficult to

reach for bulk density measurements, and the bulk density in alluvial deposits is generally variable. Here, we use an estimated bulk density for starting alluvium of 1.9 g cm^{-3} (30% porosity; estimated variability of ±20%, see below). If the addition of the immobile element in dust is accounted for, the equation for strain includes a mass scaling factor:

$$\varepsilon_{i,w} = \frac{\Delta_v}{V_p} = \frac{V_w - V_p}{V_p} = \frac{V_w}{V_p} - 1 = \left[\frac{\rho_p C_{i,p+d}}{\rho_w C_{i,w}} \times \frac{m_p + m_d}{m_p}\right] - 1 \quad (9b)$$

From Eq. (9b) it is clear that a separate means of distinguishing dust from parent material is needed to correctly quantify volumetric strain. When the mass of dust inputs is large relative to that of parent material, Eq. (9a) will underestimate the value of volumetric strain. In other words, where the mass of dust relative to parent material is significant, Eq. (9a) will overestimate the magnitude of collapse relative to the parent alluvium (i.e., when $\varepsilon < 0$), and underestimate the value of expansion (i.e., when $\varepsilon > 0$). An apparent volumetric collapse is essentially relative to total silicates (dust plus alluvium) and likely reflects in situ weathering of silicate dust, even as the total soil volume may have actually increased relative to starting alluvium due to silicate dust addition. Thus a comparison of volume and mass changes relative to total silicates is useful for considering the long-term net effects of total silicate weathering (both in situ geologic substrate and added dust) vs. atmospheric solute additions in soils on hyperarid landscapes.

2.5.3. Uncertainty in mass balance calculations

In deriving total and elemental mass gain or loss values relative to a mass in parent material or soil, the greatest source of uncertainty can be the nature of the parent material (Riebe et al., 2003). This affects concentration values for specific elements in parent material (immobile element "*i*" and element "*j*") and is difficult to quantify, as parent material is often characterized by evaluating a similar but perhaps not identical material. Here, we have assumed that soil gravels represent parent alluvium, and that silicate dust is identical in composition to soil gravels. We observed variation in [Zr] of 27% (1 standard deviation) among gravel samples from multiple horizons at all three sites, and variation of 30% among samples of all candidate parent materials (gravel, dust, and wash fines; Table 2). Variation among gravel samples and within soil samples for higher abundance elements (Si, Al, Na, Ca) was generally less than 10%. For total mass gain or loss values relative to mass of the parent material (T; Eq. (4)), standard error propagation using these values (Harris, 1995) results in uncertainties that vary with the magnitude of T (Eq. (4)), but generally are higher for values of T closer to zero. Calculation of total mass gain on an area basis (M, Eq. (5)) adds uncertainty associated with soil bulk density measurements (uncertainty of 10% based on observed variation), and is also higher for values close to zero. Volumetric strain calculations (ε values, Eq. 9) contain additional uncertainty due to likely variation in the bulk density of parent alluvium (estimated as ±20% for silty to gravelly texture). For depth-integrated values, error propagation may increase or reduce uncertainty compared to individual horizon values. Here, calculated uncertainty values are included with results.

It is important to note that this study does not address spatial variability within climate zones. However, we suggest that our estimated uncertainties provide a useful preliminary guide for evaluating differences among sites, and for considering uncertainties that generally arise in soil mass balance calculations.

3. Results and discussion

3.1. Landform ages

For the Yungay (driest) site, single crystal $^{40}Ar/^{39}Ar$ analysis of sanidine grains within ash samples provides a precise maximum age for a nearby, correlative fan surface (Table 3). For ash sample Yungay-02-UL, ages for 11 out of 15 grains form a symmetrical distribution with an acceptable scatter (i.e., equal to analytical error; MSWD = 1.5) around a weighted mean age of 2.14 ± 0.05 Ma. Four grains were eliminated from the calculation of the mean, one with an apparent age significantly younger than the main cluster (probably due to alteration) and three with older apparent ages, which may have been inherited from older ashes. For sample Yungay-02-L, ages for eight out of 11 grains form a symmetrical distribution with an acceptable scatter (MSWD = 1.5) around a weighted mean age of 2.10 ± 0.05 Ma. Three grains with ages significantly younger than the main cluster, again probably due to alteration,

Table 3
Landform age estimates based on dating of buried volcanic ash and cosmogenic nuclide exposure ages of surficial boulders (methods described in text)

Site	Maximum age using $^{40}Ar/^{39}Ar$ of buried ash (Ma)	Exposure time using in situ ^{10}Be and ^{26}Al in surface boulders (Ma)	Exposure age using ^{21}Ne in surface boulder (Ma)	Erosion rate (m Ma^{-1})
Yungay	2.1 ± 0.1[a]	2.12 ± 0.05		0.160 ± 0.014
Altamira-1		>3.9 ± 0.1	9–14	0.054 ± 0.004
Altamira-3		<4.4 ± 0.3		0.204 ± 0.228
Copiapó		2.3 ± 0.4		0.175 ± 0.039

[a] Ash sample is from a separate, correlative fan surface.

were excluded from the calculation of the mean for this sample. The mean ages for the two samples, 2.14 ± 0.05 and 2.10 ± 0.05 Ma, respectively, agree within errors, consistent with their stratigraphic proximity within the fanglomerate. The ash dates provide a maximum age for the overlying fan surface, and by correlation, a maximum for the surface containing the Yungay soil.

Cosmogenic nuclide results provide information on both minimum exposure ages and maximum rock erosion rates (Table 3, Fig. 3). These results are shown in Fig. 3 along with other samples from the Atacama Desert examined by Nishiizumi et al. (2005). Isochrons of ^{10}Be and ^{26}Al evolution indicate that the boulders at all sites have experienced exceedingly low rock erosion rates and are approaching isotopic steady state (where production is equal to loss through decay and erosion) (Table 3; Fig. 3; Owen et al., 2003). Rock erosion rates vary from 0.054 ± 0.004 m Ma^{-1} (Altamira-1) to 0.175 ± 0.039 m Ma^{-1} (Copiapó) and are among the lowest reported on Earth (Nishiizumi et al., 1991; Nishiizumi et al., 2005). Exposure ages range from 2.12 ± 0.05 Ma at Yungay to $>3.9 \pm 0.1$ Ma at Altamira (Table 3). While these results provide minimum exposure times for the boulders, their proximity to steady state (Fig. 3) suggests that exposure times may be longer than those calculated using ^{10}Be and ^{26}Al (Table 3).

Altamira-3 (Table 3) lies outside of the no erosion/steady-state erosion window shown in Fig. 3, indicating that it has experienced a complex exposure history and its calculated exposure age (4.4 ± 0.3 Ma) may be greater than the age of the landform. Altamira-1 ($>3.9 \pm 0.1$ Ma) and Copiapó (2.3 ± 0.4 Ma) fall within or near the no erosion/steady-state window shown in Fig. 3, indicating that they have been subject to continuous exposure. Their proximity to the far corner of the erosion/steady-state window means that they lie close to secular equilibrium of ^{10}Be and ^{26}Al, and should be interpreted as minimum ages for these landforms (Table 3, Fig. 3).

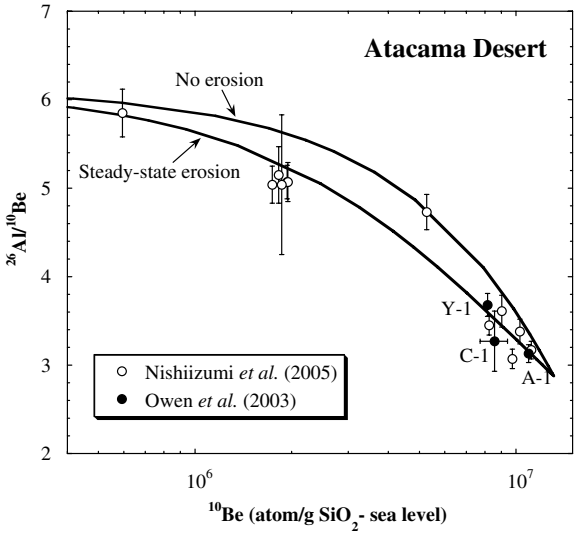

Fig. 3. Cosmogenic radionuclide results for surficial boulders at Yungay (driest, Y-1), Altamira (intermediate, A-1), and Copiapó (arid, C-1) sites. Open circles represent landforms in the southeastern Atacama Desert.

Further analysis of Altamira-1 for ^{21}Ne indicates an exposure age of 14 My, calculated using the average erosion rate from the ^{10}Be and ^{26}Al analyses, and a minimum exposure age of 9 My assuming no erosion (an unlikely scenario). This exposure age is much greater than the Quaternary age mapped by the geological survey (Naranjo and Puig, 1984). It is likely that this boulder experienced significant exposure prior to deposition on the landform, and is ultimately derived from erosion of the Miocene age Atacama Gravels found upstream from the site (Naranjo and Puig, 1984). Thus the exposure time of this boulder likely does not reflect the age of the geomorphic surface upon which it currently rests. However, the landform is stratigraphically lower than the Atacama Gravels, but higher than the current wash, and hosts soils very high in sulfate. Therefore it is likely to be Pliocene in age.

At Yungay, our landform age results and field observations suggest that major fluvial incision and deposition ceased near the Plio-Pleistocene boundary, as rainfall became insufficient to generate runoff and drive these processes. This apparent termination of the most recent major fluvial episode in the Yungay region coincides with (a) changes in sediment stratigraphy and chemistry to the north that indicate the most recent transition to hyperarid conditions (Hartley and Chong, 2002); and (b) strengthening of subtropical upwelling systems globally and in the eastern Pacific, associated with global cooling in the late Pliocene (Ravelo et al., 2004; Wara et al., 2005). Subsequent, ongoing hyperaridity would allow these near-level landforms to accumulate the ongoing rain of atmospheric salts and dust.

3.2. Atmospheric composition, deposition rates and sources

We hypothesized that with increasing aridity, atmospheric inputs to soils become a critical component of the soil mass balance. In this section, we consider the composition of airborne particles and atmospheric deposition at the three sites, and compare it to the composition of the driest soil, in order to evaluate: (1) the variation of atmospheric inputs among sites, (2) the relationship between inputs and the integrated quantities of salts in the hyperarid endmember soil, and (3) likely sources of atmospheric materials deposited to soils. At all sites, we find evidence of both marine and salar-derived solutes in atmospheric deposition to soils, as well as silicate dust inputs containing clay minerals.

Solute concentrations relative to Na^+ provide a means of comparing solute composition among samples, independent of sample size. The composition of airborne particles ("total airborne") and atmospheric deposition ("all dust") relative to Na was similar at all sites (error bars in Fig. 4a). Water-soluble salts comprised $44 \pm 15\%$ of total airborne particle mass, and $37 \pm 22\%$ of total deposited mass. Na

and Cl accounted for 10–15% of total mass in air and dust samples, suggesting a significant sea salt component (20–30%). Na and Cl were primarily present in coarse particles (>2.5 μm) at the coastal site (Fig. 4c and d), as expected for sea salt. At the inland site, this was true for Cl but not Na (Fig. 4b). Coastal airborne particles had about 10-fold more Na and Cl in the coarse fraction (Fig. 4c), suggesting that ~90% of coarse sea salt may be deposited as airborne particles are transported inland.

For water-soluble salts, soil-based deposition rates (Table 4) were calculated using the ion inventories and elemental mass gains for the Yungay profile, divided by the maximum landform age (2.1 My). This unique measure of very long-term deposition rates is only valid for sites like Yungay, where the distribution of salts with depth is strong evidence of minimal leaching losses below our two-meter excavation (see soils discussion, Section 3.3). These soil-based deposition values are generally lower than directly measured deposition rates from the dust traps, with the exception of Ca (Table 4). Soil-based rates for chloride, the most conservative species in terms of in-soil processing, are close to measured deposition rates (Table 4) and in good agreement with rates measured or assumed elsewhere (Tyler et al., 1996). Given this reasonable result for chloride, the low soil-based nitrate deposition rate (Table 4) and nitrate:sodium ratio (Fig. 4a) may indicate gaseous rather than dissolved loss of nitrate from the soil.

In air and deposition samples, as well as in the Yungay soil, Na was equimolar within error with nitrate plus chloride, suggesting formation of nitrate from NO_x on sea salt particles and substitution of nitrate for chloride (Seinfeld and Pandis, 1998; Michalski et al., 2004). Airborne and deposition nitrate and sulfate (vs. Na) were elevated compared to bulk seawater at all sites (Fig. 4a), similarly suggesting nitrate and sulfate formation via atmospheric chemistry. Elevated nitrate, sulfate, Na and Ca in Yungay dust samples relative to the other sites (Table 4) may reflect enhanced anthropogenic activity currently (local iodine mining and copper smelting). However, the long-term deposition rates determined from the Yungay soil inventory were up to 50-fold lower than the lowest dust samples (Table 4), perhaps indicating oversampling by the traps or increased contemporary dust production (see below for Si). Although deposition rates are generally lower based on the soil, the overall composition of measured deposition resembles the soil composition at Yungay only when

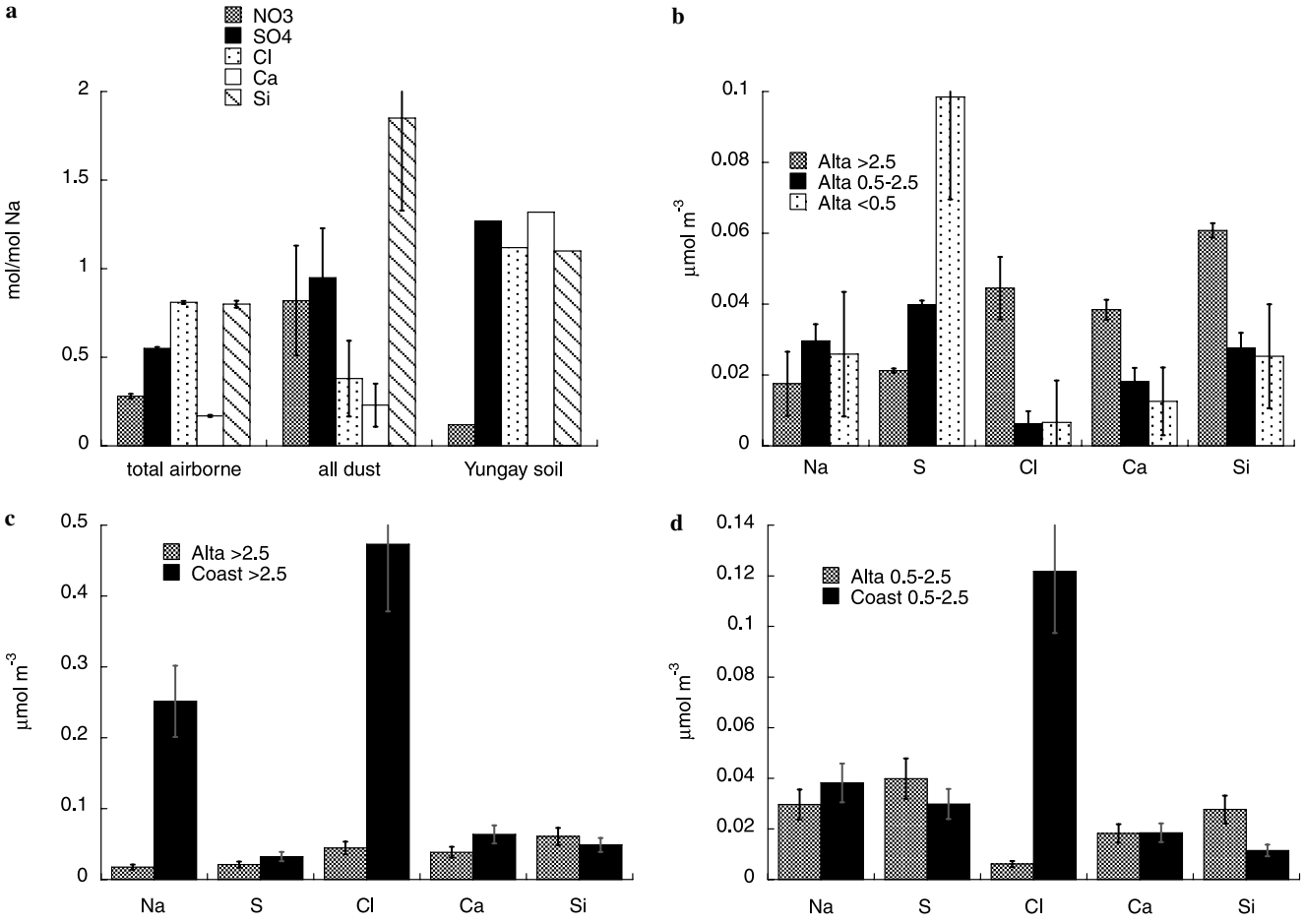

Fig. 4. Airborne, dust and soil chemistry: (a) ratios to Na at the driest site, (b) aerosol size fractions at the intermediate rainfall site (diameters in μm), (c) comparison of inland (Altamira) vs. coast site coarse fraction (>2.5 μm), (d) comparison of inland vs. coast site fine fraction (0.5–2.5 μm).

Table 4
Air-to-soil fluxes of Si and select ions (mmol m^{-2} y^{-1}) based on passive deposition samplers (top three rows) and from soil inventory divided by soil age (last row)

	Total (g m^{-2} y^{-1})	Si	Na^+	Ca^{2+}	Cl^-	NO_3	SO_4
Yungay annual ($n = 2$)	4	22	20	6	4	17	19
Altamira annual ($n = 2$)	2	29	11	1	8	12	13
Copiapó annual ($n = 2$)	2	25	12	2	4	6	8
Mean annual ($n = 6$)	4 ± 2	25 ± 4	14 ± 6	3 ± 2	5 ± 2	12 ± 5	13 ± 5
Net geologic rate[a] (Yungay soil)	0.4 ± 0.3	<6[b]	1.1 ± 0.2	1.5 ± 0.2	1.2 ± 0.2	0.13 ± 0.01	1.4 ± 0.2

[a] Soil-based rate for species other than nitrate is net elemental or total mass change (Δm/A) in the Yungay soil to a depth of 1.5 m, normalized to immobile element concentrations (Zr) and divided by surface age (2.1 My) based on age constraints discussed in text.
[b] Maximum soil-based rate based on total fine fraction (<2 mm) inventory divided by surface age (2.1 My).

whole-soil salt inventories are considered (Fig. 4a). This suggests downward transport and vertical separation based on solubility, even within the driest soil, and indicates that the samplers were successful in capturing overall deposition, rather than just remobilized surface soil.

3.2.1. Nitrate

The soil-based nitrate deposition rate (0.13 mmol m^{-2} y^{-1}; Table 4) is 100-fold lower than measured deposition, and 10-fold lower than pre-industrial rates estimated by Michalski et al. (2004) for this region. The soil-based rate may be affected by in situ additions and losses, as well as measurement uncertainty, though we hypothesize that these uncertainties cannot account for more than an order of magnitude discrepancy. We suggest that the soil-based rate should be a better estimate of long-term deposition rates than a year of accumulation in a passive trap.

Pre-industrial N deposition rates have been estimated (Michalski et al., 2004) based on regional source modeling (Holland et al., 1999). However, natural sources of N deposition in this region are not well understood. Continental sources may include Amazonian biomass burning, volcanic emissions (Mather et al., 2004a,b) and gaseous losses from more productive soils to the south. Marine production of reactive N in biologically productive upwelling zones is poorly quantified but thought to be low (Galloway et al., 2004). However, marine production of NO_x by photolysis (of dissolved nitrate, nitrite) has been observed in unpolluted, remote settings (e.g., Torres and Thompson, 1993) and is likely to occur to a greater degree in this area given elevated seawater nitrate (~10 ppm) and upwelling waters near our sites (Marín and Olivares, 1999). In addition, nitrate may be derived from photolysis of marine organic N at the ocean surface and in fogwaters (Zhang and Anastasio, 2003). Biogenic generation of alkyl nitrates ($RONO_2$) and NH_3 are additional photolytic precursors of NO_x that are likely to be elevated in upwelling zones, but are not well understood (Seinfeld and Pandis, 1998; Chuck et al., 2002; Moore and Blough, 2002). Given these uncertainties, hyperarid soils provide a useful long-term indicator of pre-industrial nitrate deposition that merits further study.

3.2.2. Sulfate and calcium

Measured sulfate deposition fluxes (Table 4) were about 10-fold higher than soil-based fluxes. Because sulfate is less susceptible to dissolved or biological losses than nitrate salts, this suggests that contemporary deposition may be higher than the long-term average, or that deposition sampling may overestimate true rates. Both measured deposition and concentrations in air samples (Fig. 4) are likely to contain fog-associated sulfate due to sampling during fog events. In the passive traps, evaporation of condensed water was evident in the patterns present on the pan walls. Fog fluxes in remote locations can significantly influence sulfate deposition rates (Bergin et al., 1995), and at our sites are expected to influence both deposition (rates and composition) and chemical transformations at the soil surface.

Sulfate levels in air samples collected by filtration (total airborne and <0.05 μm fraction, Fig. 4a and b) are likely elevated as a result of chemical reactions on the filter (reaction of SO_2 on particles) and thus are an artifact of sampling to some degree. However, they indicate SO_2 chemistry that may occur at the soil surface when sea salt is deposited (Michalski et al., 2004; Quinn et al., 2005). Measured SO_2 levels near the Yungay site (~5 ppb; Quinn et al., 2005) are high enough to explain observed sulfate levels in filtration samples given the air volumes sampled (20–40 m^3). Although a copper smelter near the Yungay site is a likely anthropogenic source of atmospheric sulfate currently, and is an additional source of error in comparing contemporary deposition to soil-derived fluxes, the soil-based values in Table 4 suggest that relatively high sulfate depositional fluxes have occurred for at least the last two million years.

As with N, strong offshore upwelling is a likely source of biogenic SO_2 (e.g., from dimethyl sulfide (DMS)), a well-known precursor of non-sea-salt sulfate and a likely component of sulfate deposition to desert soils near upwelling zones (Eckardt and Spiro, 1999; Yvon and Saltzman, 1996), including the Atacama Desert (Rech et al., 2003). Likely marine layer DMS concentrations in this area are on the order of 500 pptv (0.025 μmol m^{-3}) (Koch et al., 1999), and sea salt scavenging of the resulting SO_2 at this level is expected to yield at most 0.005 μmol m^{-3} sulfate

(Yvon and Saltzman, 1996), a value that is comparable to the lowest observed concentrations at our sites (0.030 ± 0.016 μmol m^{-3} sulfate). Thus, considering sulfate alone and given the limited sampling presented here, marine emissions may be sufficient to account for long-term sulfate deposition at these sites.

Ca levels in both air samples and the Yungay soil also exceed levels expected for sea salt (relative to Na, Fig. 4a), but unlike sulfate, Ca is not added to airborne particles through atmospheric chemical processes (Seinfeld and Pandis, 1998). In the Yungay soil, Ca is primarily balanced by sulfate (Fig. 4a). However, in sized air samples collected by impaction at Altamira, Ca balances only about half of the S in the fine fraction (0.5–2.5 μm; Fig. 4c), and exceeds sulfate concentrations in the coarse fraction (Fig. 4b), suggesting that Ca and sulfate are not completely coupled in airborne particles. In a previous study further north and inland, a similar pattern was observed (although concentrations were lower) in samples of sized airborne particles, collected in 17-day samples over a 31-month interval, (Rojas et al., 1990). Here, while submicron sulfate could not be well quantified due to likely sampling artifacts discussed above, low Ca relative to S in the fine fraction suggests that the sulfate present is likely balanced (in charge) by ammonium or Na (Seinfeld and Pandis, 1998). This implies that airborne sulfate is present in two forms: (1) submicron $(NH_4)_2SO_4$ or Na_2SO_4 particles and (2) $CaSO_4$ particles larger than 1 μm. Additional Ca is likely also present as $CaCO_3$ in larger particles (Fig. 4b). These larger $CaCO_3$ and $CaSO_4$ particles may represent some amount of local redistribution of surface soil, as discussed in the next section for Si, but they may also signal regional transport of salar salts (Rech et al., 2003), in addition to biogenically elevated $CaCO_3$ in sea salt (Moore et al., 2002). Notably, Ca in coastal vs. inland aerosols was decreased somewhat in the inland coarse fraction (Fig. 4c) and was unchanged in the fine fraction (Fig. 4c and d), suggesting limited deposition of marine $CaCO_3$ during transport, or terrestrial sources at inland locations. Transport of salar salts over the lifetime of the landform has likely contributed to the quantities of Ca present in the Yungay soil, which are consistent within error with rates based on passive traps (Table 4). Thus, the size distributions of airborne Ca and S suggest a mix of a persistent sea salt/marine component with other sources, including redistribution of salar salts, and indicate that Ca and S are partially decoupled in atmospheric particles deposited to these soils.

3.2.3. Ammonium

A notable difference between airborne chemistry and soil chemistry is the contribution of ammonium (not measured in deposition samples). In total airborne particulate samples at all sites, ammonium concentrations (0.024 ± 0.008 μmol m^{-3}) were equal to nitrate concentrations (0.013 ± 0.009 μmol m^{-3}). Ammonium is also comparable to nitrate (0.10–1.2 μmol g^{-1}) in surface horizons at all sites. In all soils, ammonium is present in surface horizons (0.2–0.4 μmol g^{-1}) but is absent or present at low levels below a few cm depth. Airborne ammonium is likely present in small (submicron) atmospheric particles and is deposited with sulfate or nitrate (Seinfeld and Pandis, 1998). However, despite large and variable quantities of sulfate and nitrate among sites (see soil results below) there is relatively little variation in the small ammonium inventories among sites (totals of 0.2–2 g m^{-2}). Since little ammonium is present in the soil, deposited ammonium must be transformed to nitrate or volatilized upon contact with water from fog or rain events (e.g., Schaeffer and Evans, 2005). If in situ oxidation of ammonium to nitrate occurs at the driest site, this would reduce the apparent nitrate deposition rate implied by the total soil nitrate inventory.

3.2.4. Silicon and clays

In inland total airborne particles at all sites (2002), Si was comparable in concentration to Na^+ (Fig. 4a). Airborne particle size fractions collected in 2004 indicate that Si was present in all fractions, but highest in the coarse fraction (>2.5 μm; Fig. 4b). Deposition (“dust”) was consistent with the coarse fraction of airborne particles, in that Si was two to three times as high as Na (Fig. 4a and b). This suggests that the coarse fraction dominates the total mass of deposition.

The mean rate of Si deposition from the deposition traps (25 mmol m^{-2} y^{-1}), multiplied by the landform age (2.1 My) implies a total dust-derived Si (1470 kg m^{-2}) that is four times higher than the total Si in the soil fine fraction (<2 mm; 340 kg m^{-2} in the upper 1.5 m) (rates shown in Table 4). The elevated deposition rates for Si may reflect increased disturbance by human activity (unpaved roads, mining, pollution effects on atmospheric chemistry), oversampling by the dust traps (remobilization minimized by trap design), or natural variability in silicate dust production (contemporary, one-year measurement vs. 2 My of accumulation in soil). This potential variability for Si deposition is difficult to extrapolate to solutes, as both sources and deposition dynamics are different for silicate particles vs., e.g., sea salt particles. However, the similar composition of airborne particles, deposition and the integrated Yungay soil profile remains as evidence that regional atmospheric sources are reflected in all three measurements.

The mass balance analysis indicates small net losses of Si from the Yungay soil ($\bar{\tau}_{Si} = -0.15 \pm 0.09$; $M_{Si} = -1.8 \pm 1.0$ kmol Si m^{-2}). These losses are calculated relative to the combined alluvium plus silicate dust, and therefore do not account for the Si influx estimated by the deposition traps. However, they do suggest that these combined soil silicates are somewhat weathered. XRD results indicated that the silicate dust (0.2–2 and 2–20 μm fractions) in deposition samples contained smectite, chlorite and kaolinite, again indicating that silicate dust particles are chemically altered. These results show that while silicate dust inputs are not constrained by our mass balance evaluation of these soils, they may add considerable mass

over time, potentially contributing more mass than the starting alluvial fines. This added mass appears to be somewhat pre-weathered; thus, the Yungay soil provides a measure of long-term, inherited chemical alteration in these soils.

In summary, atmospheric deposition to these soils is similar among sites, with a composition suggesting a pervasive marine component (Na, Cl, N, S), as well as a fraction that may be salar derived (Ca, S). The contribution of silicate dust may be substantial, but it is unconstrained by the Yungay soil mass balance due to chemical similarity to parent alluvium (i.e., immobile element content). The composition of atmospheric deposition also resembles the depth-integrated composition of the Yungay soil, confirming the long-term importance of these fluxes. Thus, regional atmospheric sources determine the geochemistry of the driest soil, which in turn represents the total flux of material into and through the more humid soils.

3.3. Soil morphology and chemistry: arid to hyperarid

In this section, we first discuss results for each soil separately, starting with the arid soil (Copiapó). This soil is similar to many North American desert soils, in which sufficient rainfall allows plants and other biological processes to play a significant role in soil geochemistry, but salt accumulation also occurs. Our discussion of the driest soil (Yungay) is the most detailed, because this site reflects geochemical processes at the hyperarid, nearly abiotic extreme. Comparison of the three sites then follows in Sections 3.4–3.6.

3.3.1. Copiapó (21 mm rain y^{-1})

Carbonate (49 kg m^{-2}) and sulfate (64 kg m^{-2}) are the dominant soluble anions in this soil (Figs. 5 and 6, Table 5a), but small amounts of nitrate and chloride are also present variably with depth (Fig. 6b). Sulfate is highest in the BCyk horizon between 107 and 117 cm (2590 ± 30 μmol g^{-1} S), where S is equimolar within error with added Ca ($\alpha_{Ca} = Ca(Zr)$ in Fig. 6c), and in the BCykm horizon between 174 and 184 cm (1400 ± 140 μmol g^{-1} S). Carbonate is most concentrated in the horizons between 15 and 117 cm (Fig. 6c; 310–690 ± 17 μmol g^{-1}) and in the Cky layer below 204 cm (1020 ± 40 μmol g^{-1}). This interfingering of these differently soluble salts implies strongly variable rainfall conditions over time, consistent with evidence that this region has been affected by episodes of semiarid conditions over the last 2 My due to the northern migration of pervasive westerly winds (Lamy et al., 2000).

Total organic C in upper meter of this soil is 1.6 kg m^{-2}, among the lowest levels observed in bioactive soils (Amundson, 2001). As is typical for desert soils, concentrations are highest but patchy in the surface horizon, where amounts in plant-associated coppice dunes (289 ± 93 μmol g^{-1}; 0.35%) and cyanobacterial colonies under quartz stones (401 ± 17 μmol g^{-1}; 0.48%) far exceed those in bare soils (43 ± 10 μmol g^{-1}; 0.05%).

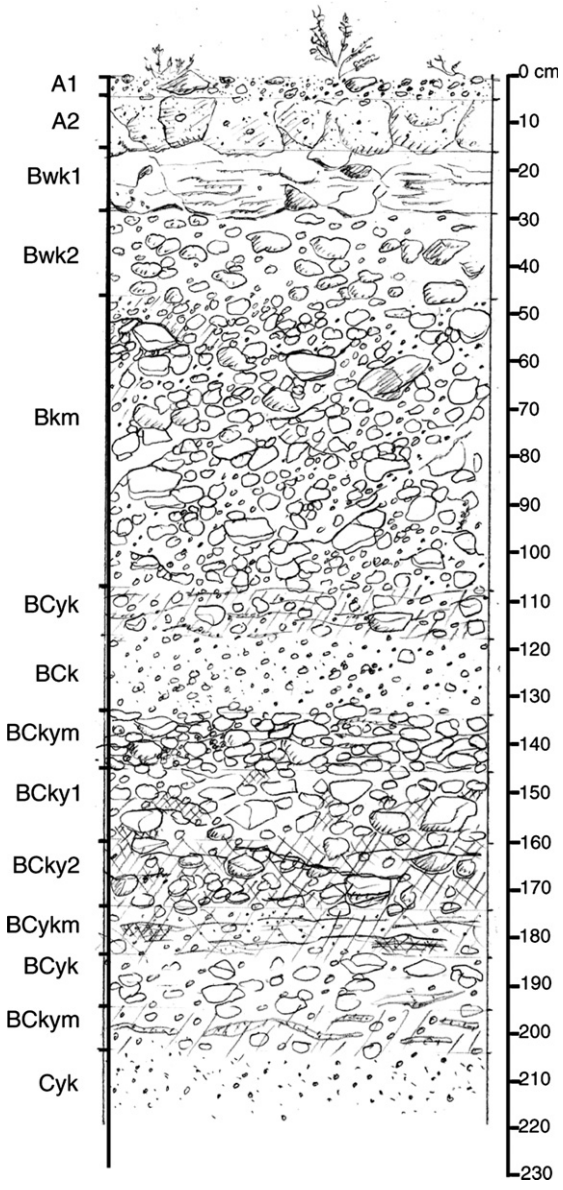

Fig. 5. A sketch of the Copiapó soil profile. Scale on right in cm. See Table 5c for description.

The mass balance analysis reveals variable apparent chemical weathering losses in this soil, with a few horizons approaching 30% loss (maximum loss of $T = -0.35 \pm 0.17$ at 9.5 cm; Fig. 6d). Losses of Na, Si, and Al vary similarly with depth (Figs. 6a and 7a), and losses of Ca are evident despite addition of carbonate and sulfate salts (Fig. 6c). Carbonate is generally not balanced by added Ca ($\alpha_{Ca} = Ca(Zr)$ in Fig. 6c), suggesting that carbonate associated Ca (and sulfate associated Ca in the horizon at 179 cm) is partially derived from chemical weathering of the parent alluvium or silicate dust. This observation is consistent with field observations of common chemically altered granitic clasts. In addition, visible reddening of the soil in the Bwk horizons between 15 and 46 cm indicates oxidized Fe. Small net gains of Fe in this soil relative to gravels (totaling 0.69 ± 0.31 kmol m^{-2}; $\tau_{Fe} = 0.50 \pm 0.22$; Fig. 7a)

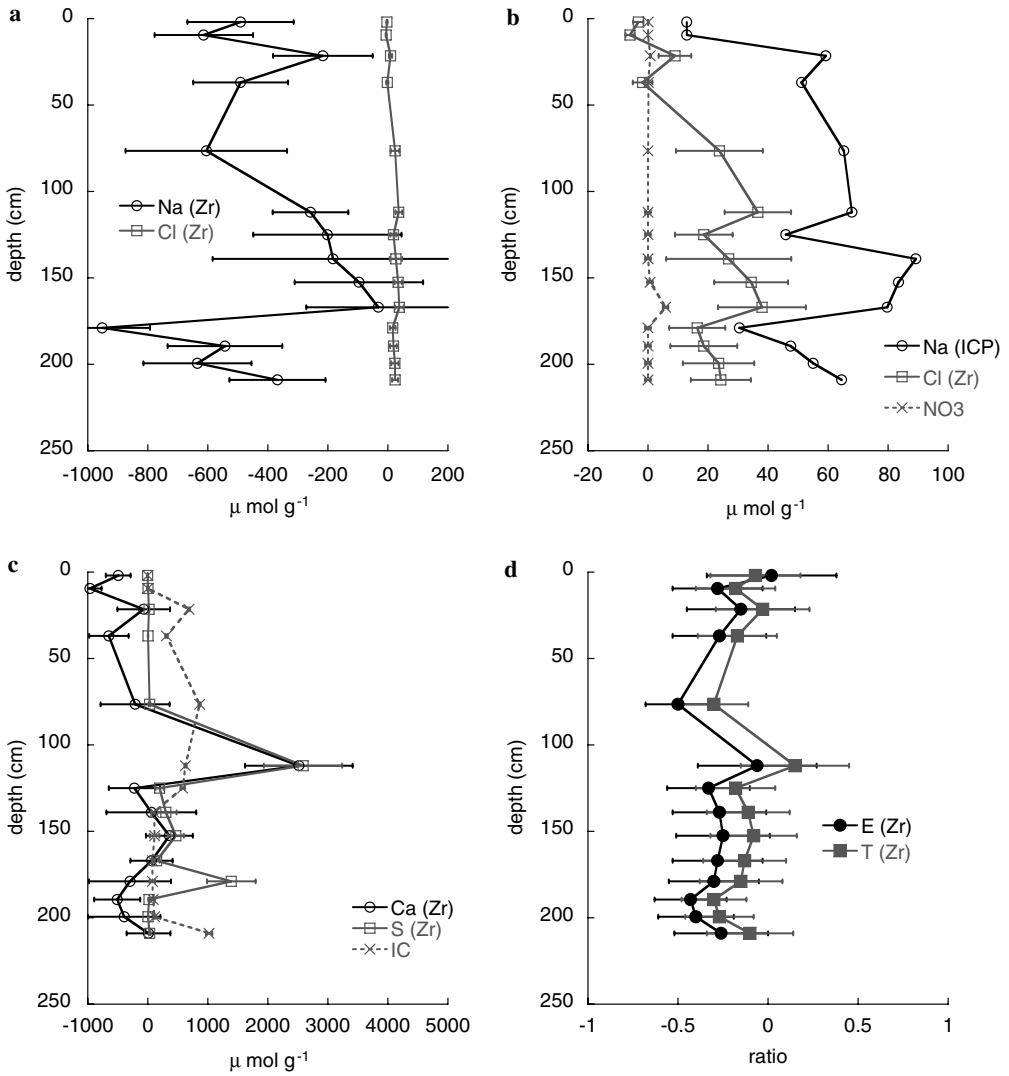

Fig. 6. Soil mass and volume change in soil with depth at the arid site (Copiapó; ~21 mm rain y^{-1}). Gains and losses of elements in most soluble (a and b), and intermediately soluble (c) salts. (d) Total change in mass (T) and volume (E). "(Zr)" indicates net elemental losses/gains relative to mass soil (α_j) using Zr as an immobile element, as described in the text. Na concentration by ICP ("Na(ICP)") included for comparison to α-values. Nitrate and inorganic carbon (IC) are directly measured concentrations. Error bars for Zr-normalized values are based on estimated uncertainties described in the text.

are consistent with elevated Fe in dust samples relative to gravel ($\bar{\tau}_{Fe} = 0.99 \pm 0.74$), suggesting that some Fe oxides may reflect dust additions, perhaps weathered in situ following deposition.

Despite net losses of Na (Fig. 6a), water soluble Na is present (Fig. 6b), and coincides with small peaks in added nitrate and chloride (Fig. 6b). These small enrichments in nitrate (maximum 5.9 ± 0.9 μmol g^{-1}) and chloride (maximum 36 ± 2 μmol g^{-1}) occur in the horizons between 15 and 174 cm (Fig. 6b; Table 5a), and suggest that episodic rain events (or longer term climate oscillations) have moved the most soluble salts down in pulses, with larger events eventually removing them from the upper few meters of soil and alluvium.

The total amount of salts retained in the Copiapó soil (170 ± 26 kg m^{-2}) is relatively small compared to the large inventories of the driest soil (830 ± 180 kg m^{-2}). This salt accumulation is counterbalanced by weathering losses, resulting in a net mass loss of -1030 ± 730 kg m^{-2} ($\overline{T} = -0.19 \pm 0.14$). Volumetric collapse ratios ($\bar{\varepsilon} = -0.30 \pm 0.07$) are similar to those for mass loss, indicating that the reduction in bulk density with soil development has been small (Fig. 6d, Table 5a). Of the weathering losses, SiO_2 accounts for -800 ± 250 kg m^{-2} or -0.009 ± 0.005 mol Si m^{-2} y^{-1}. This Si loss rate is lower than similarly evaluated rates in wetter soils of comparable age, including a semiarid California grassland soil (0.08 mol m^{-2} y^{-1}; Stonestrom et al., 1998). This low Si loss rate suggests that climate fluctuations have been modest over the lifetime of this soil, and that this soil follows the general trend of decreasing weathering losses with decreasing rainfall (Stonestrom et al., 1998; Riebe et al., 2004). Given the substantial influx of silicates indicated by deposition measurements, and the limited chemical alteration prior to deposition implied by results for the Yungay soil (-110 ± 60 kg SiO_2 m^{-2}), the calculated net mass loss in

Table 5a
Soil descriptions and selected X-ray diffraction data for the Copiapó site

Site: Copiapó					Location: S27°01.279′ W70°17.672′			
Landform and parent material: alluvial fan of granitic composition					U.S. Taxonomic classification: sandy-skeletal, mixed, thermic, shallow Typic Petrocalcid			
Slope 2%		Elevation 1215 m			MAP 20 mm			MAT 16 °C
Horizon	Depth (cm)	Bulk density (g cm^{-3})	Texture (clay %)[a]	Gravel (% by volume)	XRD[b] < 2 mm fraction	pH	Structure	Other comments
A1	0–4	1.5	lfs (1)	5	Q, AT	7.9		
A2	4–15	1.9	lfs (1)	5	Q, AT	8.0	Moderate prisms, 10 cm diameter	Eolian
Bwk1	15–28	1.9	lcos (5)	2	AT, Q, C	7.8	Strong plates, 5–10 mm; strong, coarse subangular blocks, (5%)	Bottom is thin clay/silt-rich layer with vesicles
Bwk2	28–46	1.9	vgrls (2)	50	AT, Q, C	8.2	Massive (loose)	
Bkm (petrocalcic)	46–107	2.3	vgrls (2)	70	AT, Q, C[c]	8.3	Massive (loose)	
BCyk (gypsic) (calcic)	107–117	2	lvcos	50			Platey	
BCk	117–133	2	lvcos	45 2–4 mm			Massive	
BCkym	133–145	2	lvcos	75 2–10 cm 10% >10 cm			Small (1–2 mm) plates	Mostly gypsum as plates or as clast coats
BCky1	145–160	2	vcos	60 2–10 cm			Massive	Some gypsum cement in matrix
BCky2	160–174	2	lvcos	50			Massive	Gypsum cemented
BCyKm (gypsic)	174–184	2	lcos	10			Small (1–2 mm) plates	Some plates well cemented; some carbonate on gravels
BCyk′	184–195	2	vcos	40			Massive	
BCkym calcic	195–204	2	vcos	30			Plates	Cemented sand lenses
Cyk″	204–	2	vcos	25 all small			Plates	Dense sand w/little gravel

For a guide to horizon designations and taxonomic classification, see Soil Survey Staff (1999).

[a] Field estimated textures.

[b] XRD results: AT, anorthite; C, calcite; Q, quartz; listed from highest to lowest amount.

[c] Amount similar to previous species in list.

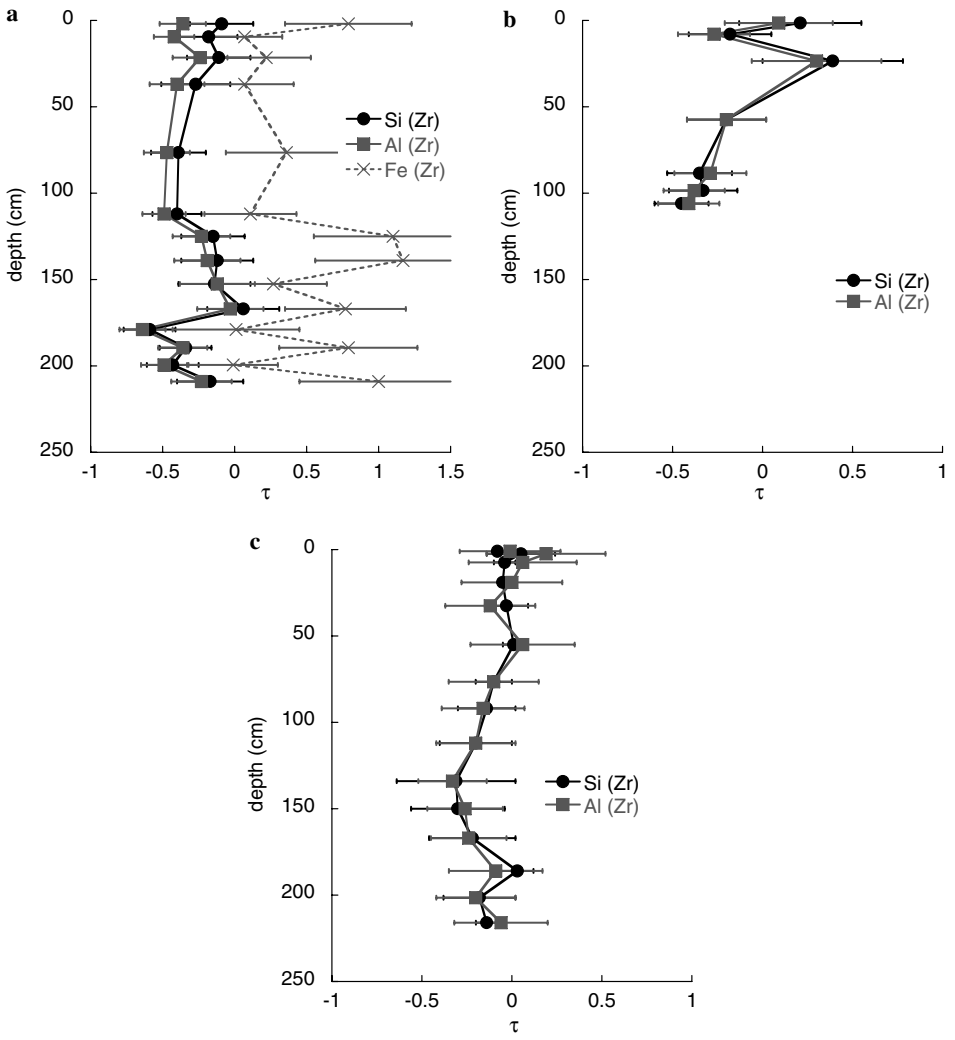

Fig. 7. Fractional elemental gains and losses in soil relative to parent material (τ) for Si, Al, and Fe at the three sites using Zr as the index element: (a) driest site (Yungay), (b) intermediate site (Altamira), (c) arid site (Copiapó).

this soil implies in situ weathering of atmospheric silicate dust following deposition.

3.3.2. *Altamira (~10 mm rain y^{-1})*

This intermediate soil is dominated by sulfate (457 kg m^{-2}) and secondarily by carbonate (35 kg m^{-2}) (Fig. 8, 9; Table 5b), with a maximum volumetric expansion (ε) of 950 ± 370% in the Bykm horizon between 13 and 34 cm (Fig. 9d). Sulfate concentrations are highest in this horizon (>4000 μmol g^{-1}, Fig. 9c), but remain high (>2000 μmol g^{-1}) to the base of the excavation. XRD analysis (Table 5b) indicates that gypsum is the dominant sulfate mineral.

Gypsum accumulation at Altamira suggests both lower average rainfall levels and smaller rain events than at Copiapó. A soft, low density gypsum horizon near the surface (Byk horizon) implies shallow accumulation, and the gypsum blocks that occur below it (Bykm) have a deeply pocketed upper boundary and are highly indurated (Table 5b). These features imply oscillations in the effectiveness of gypsum leaching—and thus rainfall—with time: a previous episode of increased rain caused disruption of near-surface morphology and consolidation and reprecipitation at depth; this was followed by more recent, shallow accumulation of near surface, low-bulk-density gypsum. In addition, the highest sulfate concentration and overall volumetric expansion at Altamira (~20 cm, Fig. 9c and d) is shallower than at Copiapó (107–117 cm, Fig. 6c), consistent with greater long-term aridity at Altamira. At the same time, the absence of anhydrite from this soil suggests that it is consistently less arid than the Yungay site.

Despite the large accumulation of sulfate, more soluble salts are present only at low levels in the Altamira soil. Nitrate reaches a maximum (3.1 μmol g^{-1}) in the Btyknm1 horizon (34–81 cm), while chloride levels are highest (50 μmol g^{-1}) in the Btyknm2 horizon (81–96 cm), but remain elevated to the base of the excavation (Fig. 9b). Thus, while observed nitrate and chloride levels are similar to those at Copiapó, we suggest that a peak in their concentration likely occurs just below the sulfate accumulation

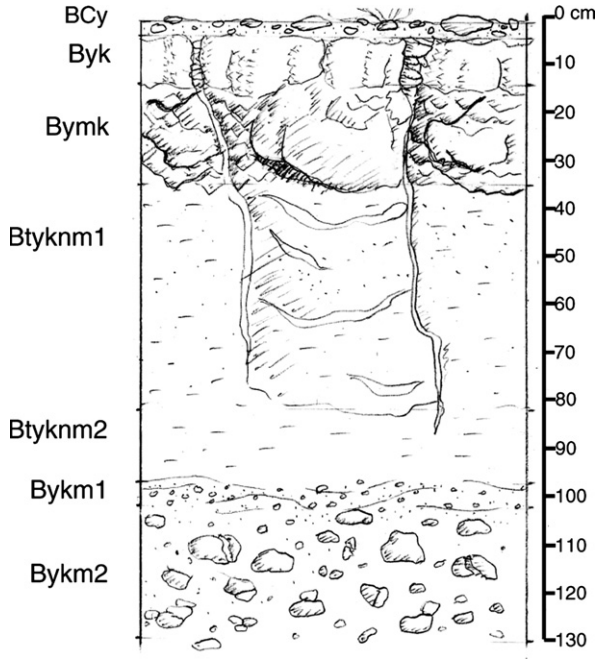

Fig. 8. A sketch of the Altamira soil profile. Scale on right in cm. See Table 5b for description.

and beyond the depth of our excavation, based on patterns of sulfate overlying nitrate/chloride observed throughout the desert (Ericksen, 1981).

In contrast with Copiapó, the mass balance for the upper ~80 cm of this soil indicates added Na (α_{Na}, Eq. (7), Fig. 9a) in excess of measured water soluble Na^+, which is close to equimolar with chloride (Fig. 9b). Assuming that no water insoluble minerals have formed, this suggests that the aqueous extraction procedure was not complete. A likely explanation is that saturation by gypsum inhibited dissolution of Na_2SO_4 (common ion effect). Therefore, the mass balance suggests that Na_2SO_4 is present at concentrations of 200–300 μmol g^{-1}. In the horizons below 80 cm depth, Na loss (Fig. 9a) coincides with small losses of Si and Al (Fig. 7b), suggesting that the silicate substrate in this soil is somewhat weathered, perhaps under previous climate conditions.

Carbonate increases gradually with depth and reaches a maximum (813 μmol g^{-1}) in the Btyknm2 horizon (81–96 cm; Fig. 9c). Organic C is low, ranging between 11 ± 2 and 19 ± 6 μmol g^{-1} (0.013–0.023%), with elevated levels occurring only in patches at the soil surface around plants (~170 μmol g^{-1} or 0.20%) and where cyanobacteria have colonized the undersides of translucent stones (210 ± 40 μmol g^{-1} or 0.25 ± 0.05%). Total organic C in the upper meter is 0.23 kg m^{-2}, an order of magnitude less than at Copiapó and quite low compared to other soils (Amundson, 2001). The decrease in both carbonate and organic C relative to Copiapó is striking, and is consistent with lower biological activity. The preferred presence of carbonate at the boundaries and in pores of gypsum blocks, and forming platy structures in the cracks between blocks, is consistent with a Ca-sulfate–carbonate system in which $CaCO_3$ is formed preferentially in low sulfate zones such as structural cracks where preferential flow occurs (Doner and Lynn, 1989). Taken together, these features indicate that the Altamira soil has experienced long-term hyperaridity marked by phases of slightly more humid conditions that do not remove sulfate, but are capable of moving it and more soluble salts deeper in the soil.

3.3.3. Yungay (<2 mm rain y^{-1})

Salt distribution with depth in the upper 146 cm of the Yungay soil follows the sequence observed by Ericksen (1981) in nitrate deposits: gypsum/anhydrite (260 kg sulfate m^{-2}) overlying a zone of halite (90 kg chloride m^{-2}) and nitratite ($NaNO_3$, 16 kg nitrate m^{-2}) (Fig. 11). In general, over the ~1.5 m depth of salt accumulation in this soil, sulfate concentrations decline dramatically with increasing depth in the upper 122 cm (Fig. 11c), whereas chloride and nitrate increase sharply in the Bnzm horizon at 122 cm (Fig. 11a and b). The considerable salt accumulation in this soil (830 kg m^{-2}) has caused a large volumetric expansion relative to the original fluvial sediment and added silicate dust (120% to 1.5 m depth; Figs. 10 and 11; Table 5c). The morphological features and depth sequence of salts in the upper 146 cm (Figs. 10 and 11; Table 5a) suggest wetting events of variable magnitude and frequency: (1) more frequent small events (rain and/or fog) that accumulate variably hydrated $CaSO_4$ near the surface (upper ~ 10 cm) and (2) larger but infrequent events that have moved more soluble nitrate and chloride salts to depths of over a meter. We discuss the processes implied by specific ions and associated morphologies in the following sections.

3.3.3.1. Sulfates: variable rainfall within a hyperarid setting.

Sulfur in the top 85 cm of the Yungay soil (where carbonate is low) is equimolar with Ca (Fig. 11c), consistent with XRD analysis showing the presence of gypsum and anhydrite (Table 5c). In the upper 39 cm, gypsum exceeds anhydrite, while below 39 cm, anhydrite exceeds gypsum (Table 5c), suggesting wetting/hydration of the upper zone. The detection of anhydrite at Yungay reflects its extreme hyperaridity, with a mean soil relative humidity of only 20% (Warren-Rhodes et al., 2006). Sulfur concentrations are highest in the Byk1 horizon (2–3 cm depth, Fig. 11c), where apparent volumetric expansion is 700% and the mass gain of salts is 250% (Fig. 11d). The S concentration in this horizon is 4470 μmol g^{-1} (Fig. 6c) corresponding to ~65% $CaSO_4 \cdot 2\,H_2O$ by weight. This very shallow, distinct and nearly pure $CaSO_4$ accumulation suggests exceedingly small wetting events, and is likely the result of relatively frequent fog events (~1 mm, many events per year; Warren-Rhodes et al., 2006). The soft prisms between 3 and 12 cm (Byk2 horizon) have a lower sulfate concentration (2460 μmol g^{-1}) and mass gain (64%) than the overlying thin horizon (Figs. 10 and 11), but their volumetric expansion remains high (370%; Fig. 11d) due to their very low

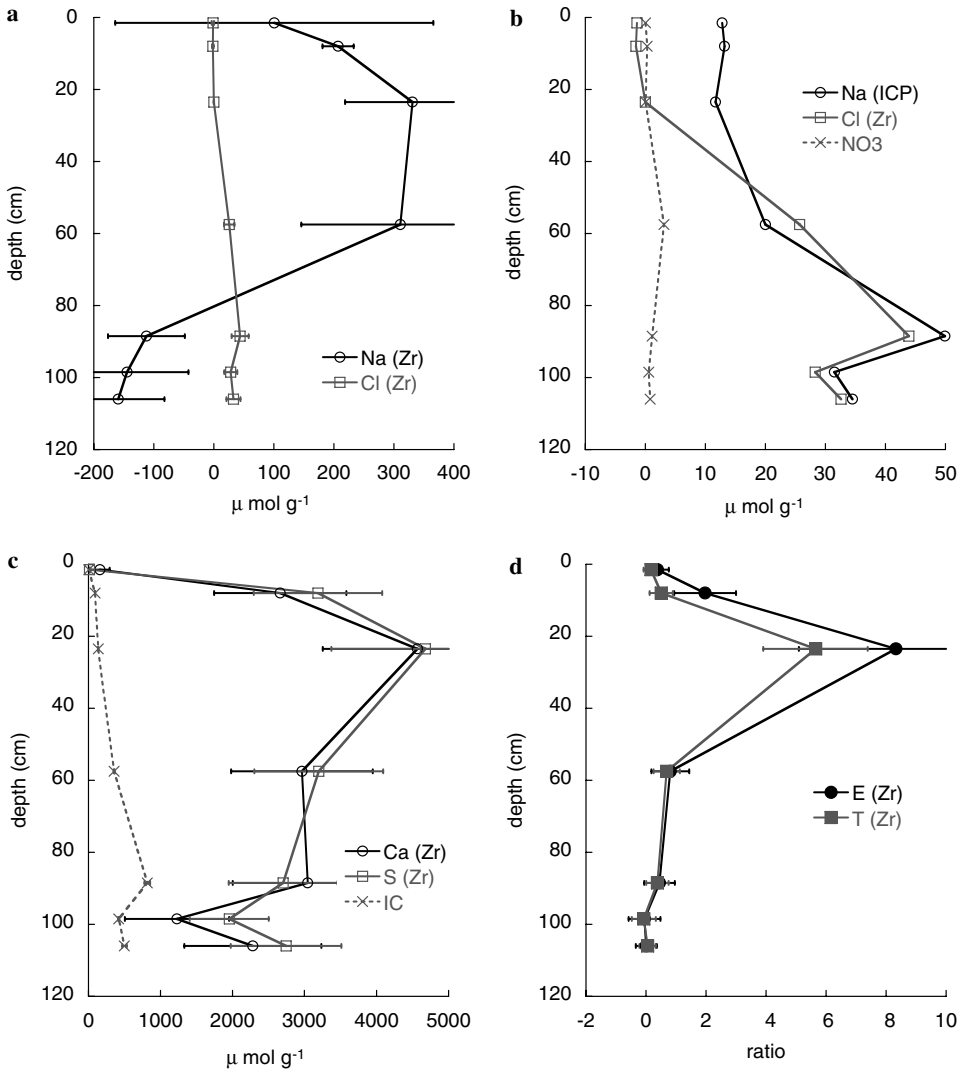

Fig. 9. Soil mass and volume change in soil with depth at the intermediate site (Altamira; ~10 mm rain y^{-1}). Gains and losses of elements in most soluble (a and b), and intermediately soluble (c) salts. "(Zr)" indicates net elemental losses/gains relative to mass soil (α_j) using Zr as an immobile element, as described in the text. Na concentrations by ICP ("Na(ICP)") included for comparison to α values. (*d*) Total fractional change in mass (*T*) and volume (*E*) using Zr as the immobile element. "(Zr)" indicates net elemental losses/gains relative to mass soil (α_j) using Zr as an immobile element, as described in the text. Error bars for Zr-normalized values are based on estimated uncertainties described in the text.

bulk density (0.6 g cm^{-3}). This low bulk density suggests that this horizon is also associated with small wetting events compared to the underlying Byk3 and By horizons (Table 5c). In these more indurated but still porous underlying horizons, higher bulk densities and more consolidated morphology suggests events large enough to dissolve, concentrate, and reprecipitate $CaSO_4$ (>10 mm), but infrequent enough to allow the overlying morphologies to re-develop. Similarly, in the extremely well-indurated Byknzm (39–71 cm) horizon, sulfate deposition over million-year timescales (based on contemporary S deposition rates) has been concentrated and consolidated by likely transport and reprecipitation with these larger rainfall events.

The presence of sulfate polygonal prisms in multiple horizons (Fig. 10; Table 5c) suggests cyclical hydration and dehydration of gypsum/anhydrite (Chatterji and Jeffrey, 1963). The threefold increase in prism width in the Byknzm horizon (39–71 cm depth; prisms 30 cm wide) relative to the overlying Byk2 horizon (3–12 cm depth; prisms 10 cm wide; Fig. 10) may be a function of decreasing evaporation rates with depth during desiccation (Goehring and Morris, 2005; Toramaru and Matsumoto, 2004). Hexagonal morphologies (~120° angles in plan view) are a common feature of both frost driven polygons (Kessler and Werner, 2003) and columnar basalts (Aydin and DeGraff, 1988) due to volume changes common to freeze–thaw, cooling and desiccation processes, with a temperature or moisture gradient driven by surface conditions (Goehring and Morris, 2005). It is possible that similar physics may drive formation of prismatic morphology with polygonal cross sections in $CaSO_4$-rich horizons of Atacama soils.

Table 5b
Soil descriptions and selected X-ray diffraction data for the Altamira site

Site: Altamira					Location: S25°45.587′ W70°11.797′			
Landform and parent material: stream terrace at toe of alluvial fan					U.S. Taxonomic classification: sandy, gypsic, thermic, shallow Typic Petrogypsid			
Slope 1%					Elevation 1012 m		MAP 10 mm	MAT 16 °C
Horizon	Depth (cm)	Bulk density (g cm^{-3})	Texture (clay %)[a]	Gravel (% by volume)	XRD[b] < 2 mm fraction	pH	Structure	Other comments
BCy	0–3	1.4	lfs (1)	15	Q, AT	7.0	None	
Byk (gypsic)	3–13	0.8	lfs (1)	0	G, Q, AT[c]	7.5	Massive and strong plates, 5–10 mm	Trans-horizon cracks containing roots and sorted, coarse sand, ~3/m
Bykm (petrogypsic)	13–34	1.2	lfs (3)	0	G, Q, AT[c]	7.7	Atrong prisms, 30 cm wide	
Btyknm1 (petrogypsic)	34–81	1.5	scl (21)	0	G, Q, AT[c]	8.1	Massive with some strong prisms, 30 cm wide (10%)	
Btyknm2 (petrogypsic)	81–96	1.6	sl (15)	0			Massive	
Bykm1 (gypsic)	96–101	1.6	cosl (8)	10% slightly >2 mm			Moderate plates, 5–10 mm	
Bykm2 (gypsic)	101–129	1.7	sl (12)	22% large cobbles			Massive	Some cobbles popped apart by gypsum crystals; otherwise gravels appear unweathered, lacking rinds

For a guide to horizon designations, including diagnostic horizon names in parentheses, and taxonomic classification, see Soil Survey Staff (1999).

[a] Field estimated textures.

[b] XRD results: AT, anorthite; G, gypsum; Q, quartz; listed from highest to lowest amount.

[c] Amount similar to previous species in list.

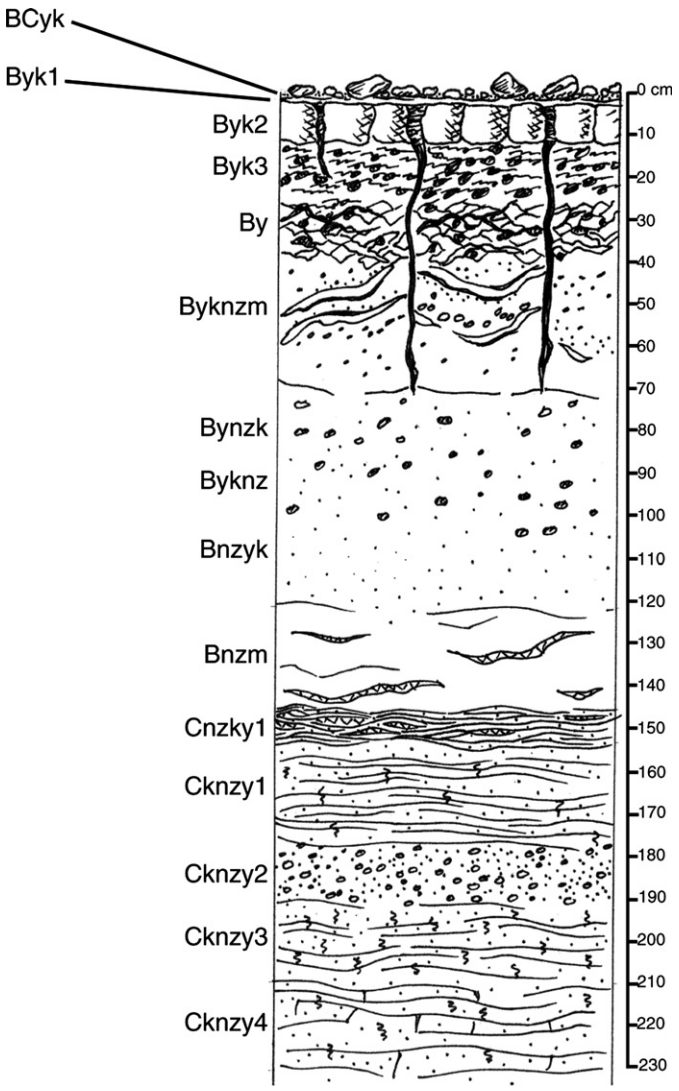

Fig. 10. A sketch of the Yungay soil profile. Scale on right in cm. See Table 5a for description.

3.3.3.2. Nitrates and chlorides: maximum rainfall events and salt distillation. Throughout the profile, Na^+ is roughly equimolar with $NO_3^- + Cl^-$ (Fig. 11a), similar to sea salt aerosols in which nitrate substitutes for chloride in halite (Seinfeld and Pandis, 1998). Nitrate increases sharply to a maximum value (470 μmol g^{-1}), along with halite (12,000 μmol g^{-1} Cl^-), at 122–146 cm in depth, where sulfate is almost entirely absent (Fig. 11a–c). 300% gains in both mass and volume in this indurated horizon (Fig. 11d) reflect salt accumulation that has added considerable mass with little change in bulk density (<10%; Table 5a). Nearly 87% of the halite and 74% of the nitrate in the entire soil is in this horizon. The similar distribution of nitrate and chloride has been observed in arid to semi-arid regions (Walvoord et al., 2003); however, the precipitation of nitrate and chloride as solids at these shallow depths indicates that wetting events have been variable but quite limited over the past 2 My.

A contributing factor to the placement of the halite-rich horizon is that it coincides with an "abrupt textural change" (Soil Survey Staff, 1999) between gravelly sands in the upper part of the soil (up to ~50% gravel in the silicate fraction prior to salt accumulation), and finer textures (27–29% clay, no gravel; Table 5c) in the lower part in the profile. As salts accumulated in this soil, this abrupt textural change may have served as a barrier to unsaturated solute transport, and likely helped to initiate retention of all soluble components within the upper 150 cm of the soil (Jury et al., 1991). The accumulation of secondary minerals is frequently observed at these textural transitions in alluvial sediments under arid to semiarid conditions (Birkeland, 1999). While not all soils in the region contain these textural contrasts, this soil is consistent with those formed from alluvial deposits throughout the region, in which a sharp decline in salt concentrations occurs within a few meters of the surface (Ericksen, 1981).

Carbonate coats on sulfate polygon sides and undersides indicates that the penetration of water and salts to subsurface horizons (below 39 cm) today is likely due to preferential flow or wetting along polygon faces, based on carbonate coats on sulfate polygon sides and undersides, following large ($\geqslant$10 cm) rain events. Following a rain event in June 2005, we observed wetting of soils between but not within these polygons. Deep (134 cm) accumulations of salts must reflect occasional larger wetting events than have been recorded to date, but estimating the magnitude of those larger events is complicated by salt accumulation with time, leading to both preferential flow paths and increasing soil thickness. Given slow and ongoing deposition at the soil surface, we suggest that multiple maximum-scale events have occurred over the lifetime of this soil.

3.3.3.3. Carbonates and organic C: biological minimum. Despite the hyperarid conditions of this region, the carbonate inventory in the Yungay soil (23 kg m^{-2} in the upper 150 cm) is remarkably low, with concentrations of 120–190 μmol g^{-1} (Fig. 11c). The low abundance of $CaCO_3$ in Atacama soils has been noted by other authors (Rech et al., 2003; Michalski et al., 2004). While $CaCO_3$ ($pK_{sp} = 8.34$) is much less soluble than $CaSO_4$ ($pK_{sp} = 4.59$), its formation is not chemically favored in this hyperarid setting. Carbonate solubility is controlled by pH, CO_2 partial pressures (P_{CO_2}), and Ca concentrations (Butler, 1982). The low organic C in the upper horizons of the soil (10–19 μmol g^{-1}) and extremely limited biological activity in the area (Navarro-Gonzalez et al., 2003; Ewing et al., 2004; Ewing et al., 2005; Warren-Rhodes et al., 2006) indicate that soil P_{CO2} levels are likely close to those of the atmosphere (360 ppm). The pH of soil equilibrated for several minutes is ~7 to 8 (Table 5a), although surface samples produce more acidic values (~5.5) upon initial wetting (Quinn et al., 2005). Calcium does not appear to be limiting, and high sulfate concentrations ($\log[SO_4^{2-}] > -3$) are likely to occur with atmospheric deposition of Na_2So_4 and $(NH_4)_2SO_4$. Under these conditions, hydrated $CaSO_4$ is the energetically

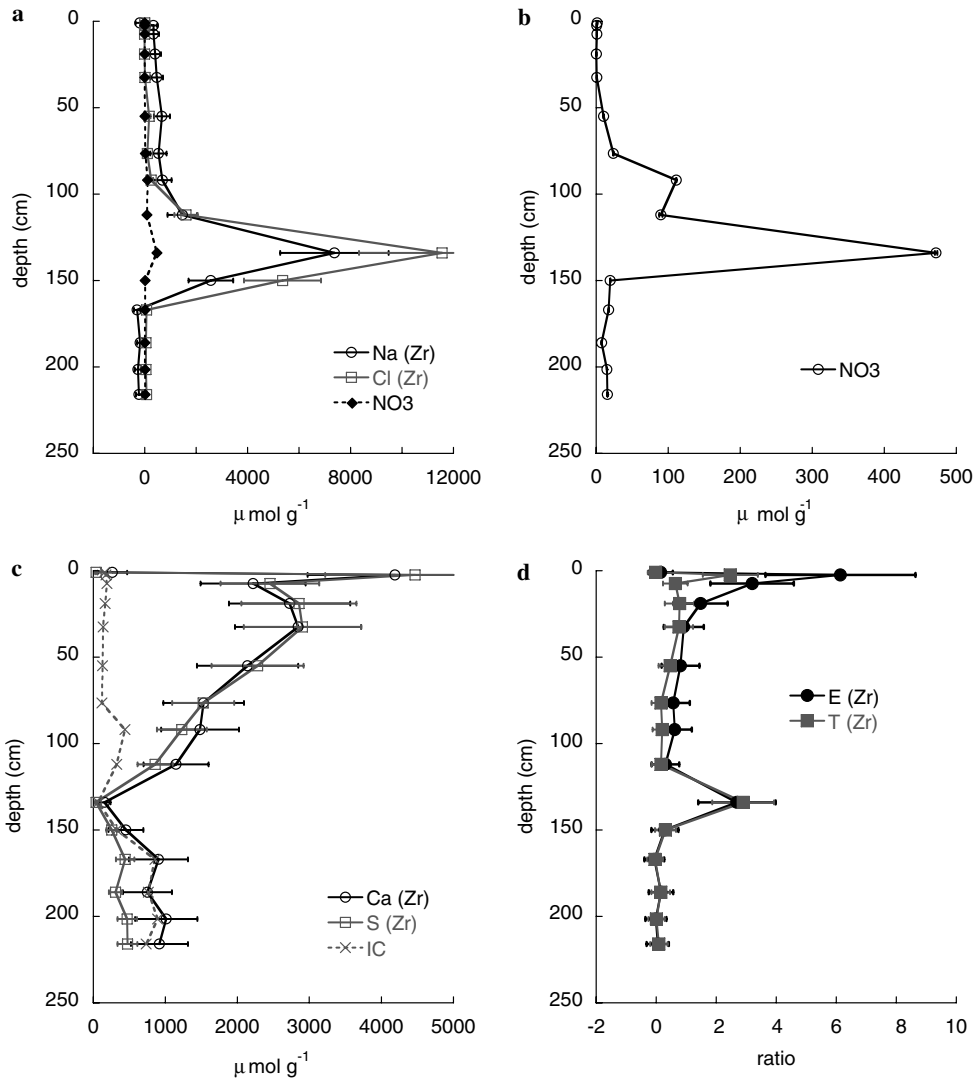

Fig. 11. Soil mass and volume change with depth at the driest site (Yungay; <2 mm rain y^{-1}). Gains and losses of elements in most soluble (a and b), and intermediately soluble (c) salts. (d) Total change in mass (T) and volume (E). "(Zr)" indicates net elemental losses/gains relative to mass soil (α_j) using Zr as an immobile element, as described in the text. Na concentrations by ICP were similar to α values. Nitrate and inorganic carbon (IC) are directly measured concentrations. Error bars for Zr-normalized values are based on estimated uncertainties described in the text.

favored equilibrium phase (Doner and Lynn, 1989), whereas $CaCO_3$ is only favored if P_{CO_2} increases and/or sulfate concentrations decline. The presence of carbonate in cracks and on prism faces suggests that preferential water flow through these flow paths is lower in sulfate or higher in pH (9–10), favoring local deposition of $CaCO_3$ (Doner and Lynn, 1989).

The relatively high carbonate content in the deep, undisturbed sedimentary strata of this soil (300–900 μmol g^{-1} below 150 cm, Fig. 11c) is likely a relict feature. It coincides with a 10-fold increase in organic C (100–250 μmol g^{-1}), the presence of relict root fragments (Fig. 10), and small apparent weathering losses of Si, Al and Na (Figs. 7c, 11a). These features suggest that a wetter period, minimally capable of supporting vascular plants, preceded the aggradation and stabilization of the landform approximately 2 My ago. In this earlier time, wetter conditions increased biological activity (leading to higher soil P_{CO_2}) and reduced sulfate activities, favoring $CaCO_3$ formation. The retention of root fragments and organic C in the lower layers attests to the low level of biological activity during the Quaternary. Sulfate concentrations of 300–500 μmol g^{-1} in these layers may reflect initial phases of $CaSO_4$ deposition following the transition to more continuous hyperaridity.

3.3.3.4. Silicate clays: pre-weathered dust additions? XRD of the clay fraction (<2 μm) in the driest soil indicates that smectite, chlorite, and kaolinite are present in the coarse (0.2–2 μm) clays of horizons found at 1, 33, and 186 cm in depth, but chlorite and kaolinite peak intensities were greater in the surface horizon (1 cm; Table 5a) and in dust than in the lower horizons. In the medium clays (0.08–0.2 μm), smectite is present in the upper horizons (1 and 33 cm) and dust, but not in the lowermost horizon

Table 5c
Soil morphological descriptions and selected X-ray diffraction data for the Yungay site

Site: Yungay Landform and parent material: distal alluvial fan of primarily granitic origin, with occasional fine grained mafic gravels			Location: S24°06.102′ W70°01.097′ U.S. Taxonomic classification: loamy, gypsic, thermic, shallow Petrogypsic Haplosalid						
Slope 1%			Elevation 1024 m		MAP 0 mm			MAT 16 °C	
Horizon	Depth (cm)	Bulk density (g cm^{-3})	Texture[a] (clay %)	Gravel (% by volume)	XRD[b] < 2 mm fraction	XRD[b] clay fraction	pH	Structure	Other comments
BCyk	0–2	1.4	15	17	Q, AT	S, M, CH, K,	7.7	Strong plates, 2 mm thick	
Byk1	2–3	0.8		1	G, AH, Q, AT		7.5	consolidated layer	
Byk2	3–12	0.6		12	G, Q, AT		7.1	Strong prisms, 5–10 cm; moderate plates in cracks, 5–10 mm	Cracks 8–10 cm apart contain soil from surface
Byk3	12–26	1.2		25	G, Q, AT		6.9	Massive	Irreversible trans-horizon cracks, ~3/m
By	26–39	1.5	11	25	G, Q, AT	S, M, CH, K	7.3	Massive	
Byknzm (petrogypsic)	39–71	1.3		10	Q, AH, G, AT[d]		7.3	Strong prisms, ~30 cm thick	
Bynzk (gypsic)	71–85	1.2		10	AH, AT[d], Q		7.4	Massive	
Byknz (gypsic) (salic)	85–102	1.2		10	Q, AH, H,[d] G, AT[d], C			Massive	
Bnzyk (salic)	102–122	1.5		0	Q, AH, H[d], C		7.3	Massive	
Bnzm (salic)	122–146	1.7		0	H, Q, N		7.2	Massive; cracks contain cubic crystals of halite	Large cavities in NaCl cement facilitate crystal growth; crystals have many shapes including fibrous, cubic
Cnzky1 (salic)	146–154	1.7	scl (27)	0				Strong plates, 1–2 mm thick	0.5–1.0 mm NaCl seams appear laterally and sub vertically through this horizon; discontinuous
Cknzy1	154–180	1.7	scl (27)					Strong plates (1–2 mm) → massive	
Cknzy2	180–192	1.6	scl (29)	<5% ~ 3 mm		M, CH, K, S[c]		moderate subangular blocks, 5–10 mm	
Cknzy3	192–211	1.7	scl (29)	0				Weak angular blocks, 1–2 cm	Patches of a white salt
Cknzy4	211–232	1.7	scl (27)	0				Sedimentary plates → weak subangular blocks, 1–2 cm	White coatings on blocks

For a guide diagnostic horizons and taxonomic classification, see Soil Survey Staff (1999).

[a] Field estimated textures.

[b] XRD results: AT, anorthite; AH, anhydrite; C, calcite; CH, chlorite; G, gypsum; H, halite; K, kaolinite; M, mica; N, nitratite; Q, quartz; S, smectite; listed from highest to lowest amount.

[c] Present in coarse clays (2–20 μm) only.

[d] Amount similar to previous species in list.

(186 cm). Because these horizons represent the upper and lower portions of this soil, these results suggest that clay minerals in this soil represent a mix from multiple sources. The clays in the lower section likely represent those deposited or formed in situ in the original alluvial deposit. The clays in the upper section may represent (a) a different alluvial source, (b) dust deposition and downward transport, (c) salt mediated clay formation, or (d) a combination of these sources. The clay minerals in deposited dust may contribute to small apparent losses of Si and Al from the Yungay soil (Fig. 7c). Overall, our results suggest that silicate dust deposition has added pre-weathered clays to these soils.

In summary, the Yungay profile has retained atmospheric deposition due to extreme hyperaridity through small, variable wetting events over the past 2 My. Total mass addition to this soil reflects regionally specific atmospheric sources (marine, salar). Independent of local/regional sources, our data indicate three processes that are generally applicable to hyperarid soils: (1) retention of most atmospheric ions, (2) reprecipitation of thermodynamically favored salt phases (i.e., different from atmospheric speciation), and (3) vertical redistribution of those phases based on solubility, within a fluvial and dust derived silicate matrix that has been preserved essentially unaltered for ~2 My since deposition.

3.4. Atmospheric deposition and Atacama soils

All landscapes on Earth receive continuous inputs of atmospheric solutes and dust, but due to rainfall and leaching, most of these inputs are not retained in soils. Our analysis of airborne particles and deposition shows that atmospheric inputs to our sites are similar, and it is weathering and leaching losses that vary with aridity: from >80% loss of deposited salts and 20% loss of total silicates at Copiapó, to effectively zero losses at Yungay. The total solute chemistry of the driest soil is similar to that of atmospheric deposition, indicating that most atmospheric inputs are quantitatively retained, and that energetically favored salts are redistributed within the soil profile based on solubility. The character and rate of inputs in the Atacama Desert are locally specific, due to proximity to marine, volcanic, and salar sources, but no location on Earth escapes the ongoing influx of atmospheric mass. At many locations on Earth over My timescales, these atmospheric additions may exceed the in situ mass of geologic substrate.

The soils examined here are strongly influenced by marine salts. However, our analysis also suggests influence by salar salts, and volcanic emissions are a likely contributor (Eckardt et al., 2001; Rech et al., 2003; Bao et al., 2004; Bao, 2005). In particular, the relative amount of soluble Ca (vs. Na) in the driest soil far exceeds that in seawater (Seinfeld and Pandis, 1998). Calcium may arrive as a mix of $CaCO_3$ and variably hydrated $CaSO_4$ in salar-derived dust, with additional marine $CaCO_3$, and possibly exchangeable Ca on clay minerals. Simultaneous deposition of $(NH_4)_2SO_4$ with $CaCO_3$ would increase sulfate concentrations and acidify pH upon wetting by rain or fog, Volatilizing ammonia. Subsequent drying would favor formation of $CaSO_4$ rather than $CaCO_3$ at sites dry enough to retain sulfate and with low enough biological activity to minimize soil CO_2. This study indicates that this $CaSO_4$ vs. $CaCO_3$ threshold occurs near 20 mm rain y^{-1} in temperate desert soils.

Previous work has demonstrated that the unusual accumulation of salts in Atacama soils—particularly nitrate and sulfate—is a function of long-term atmospheric deposition in a hyperarid climate (Michalski et al., 2004). This study shows that the most hyperarid soils retain a characteristic suite of atmospheric salts that is apparent only when trends with depth in the soil are considered. Local atmospheric chemistry dictates the character of these salts, and the salt composition of hyperarid soils should vary predictably by location.

This finding is particularly relevant to Mars, where generation of atmospheric particles likely occurs through volcanic activity, limited oxidative capacity in the atmosphere, extreme aridity and extensive eolian transport and alteration (Thiemens et al., 2001). These processes might be expected to produce a suite of salts in Martian soils that is geochemically distinct from the Atacama in key ways, but is similarly related to atmospheric composition, and similarly redistributed with depth by limited wetting.

3.5. Soil based evidence of climate change and variability

Soils are historical bodies that retain climate change information in both chemical and morphological features. The stability of landforms in the Atacama Desert has resulted in extensive ancient soils that are potentially valuable records of climate history for the region. At all of the sites we examined, soil morphology and chemistry suggest some degree of climatic oscillation over time. These signals generally weaken as rainfall decreases. In the lower meter of the arid Copiapó soil, alternating peaks of $CaSO_4$ and $CaCO_3$—which have distinct solubilities—and variably enriched Fe (Figs. 6c and 7a), may correspond to more frequent or intense variation of rainfall levels (and thus leaching depths) compared to sites to the north. This variation most likely has been a function of periodic northward migration of westerlies carrying winter rain from the Pacific (Lamy et al., 2000). Further north at Altamira, in the present hyperarid zone, evidence of extensive gypsum dissolution and reprecipitation at depths well below those expected from recent rainfall levels indicates somewhat wetter episodes in the past. At the driest site, accumulation and limited redistribution of halite and nitratite below gypsum and anhydrite imply rain events larger than those observed today. These events must be sufficiently frequent to produce distinct, solubility driven zones of accumulation a meter below the surface despite ongoing deposition at the surface (Fig. 11). At the same time, distinct near-sur-

face prismatic morphologies in gypsum and anhydrite indicate consistently hyperarid conditions; these morphologies are disrupted at the intermediate site, where conditions are only slightly more humid, but currently still hyperarid. In the Yungay soil, rainfall increases in the last 2 My have not been sufficiently large or sustained to alter the key feature of hyperarid soil formation: accumulation and limited redistribution of atmospheric solutes as precipitated salts within a few meters of the landscape surface. This 2 My timeframe is consistent with global scale shifts in climate (Ravelo et al., 2004; Wara et al., 2005).

3.6. A pedogenic threshold in soil chemistry with limited rainfall

This work shows that soil formation is fundamentally changed at the arid-hyperarid transition, with a shift in the sign of total mass balance from negative to positive (Fig. 12a). In the Atacama Desert, the transition to retention of atmospheric solutes occurs where rainfall levels are currently less than 20 mm y^{-1}. Compared to net mass loss ($\overline{M} < 0$) of -1030 ± 760 kg m^{-2} at Copiapó, the mass balance in the Altamira and Yungay soils has shifted from slow weathering losses to continuous accumulation of salts ($\overline{M} > 0$) totaling >800 kg m^{-2}. In wetter climates, biological activity and mineral hydration lead to substantial volumetric expansion (up to >500%) in younger soils (<10^5 y), but collapse dominates after ~10^5–10^6 y (Chadwick and Goldstein, 2004). Among ancient soils (>10^6 y), these hyperarid soils have undergone a greater degree of long-term volumetric expansion ($\overline{\varepsilon} > 100\%$) and associated mass gain ($\overline{T} \sim 60\%$) than has been quantified elsewhere on Earth (Capo and Chadwick, 1999; Amundson, 2004; Chadwick and Goldstein, 2004). Moreover, the mechanism of expansion is fundamentally different in hyperarid soils: accumulation of atmospheric mass. This study is the first to characterize this transition from wetter soils formed by net loss of mass through long term chemical weathering and

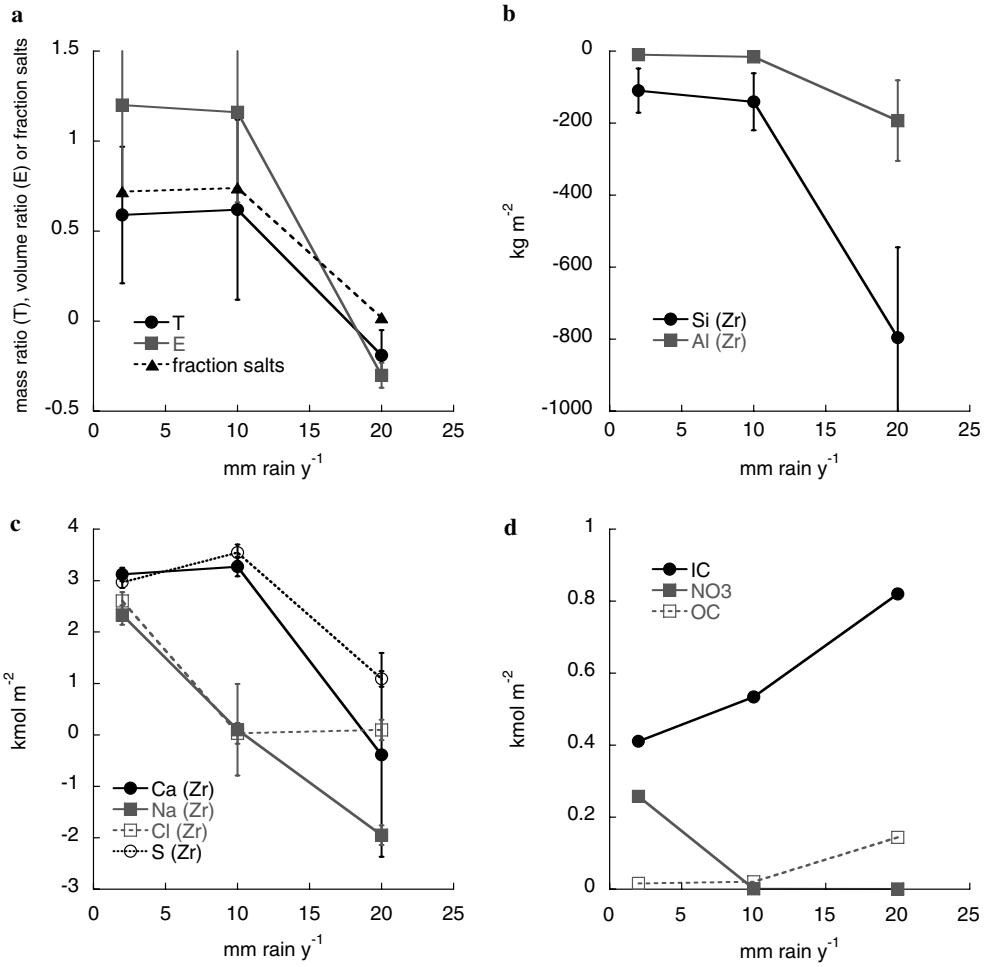

Fig. 12. Total mass change, volume change, and elemental changes in soils vs. parent material as a function of rainfall. "(Zr)" indicates index element for calculating net elemental changes relative to soil mass (M_j). Mass Si and Al refer to the oxide forms (SiO_2 and Al_2O_3, respectively). IC is inorganic carbon, OC is organic carbon.

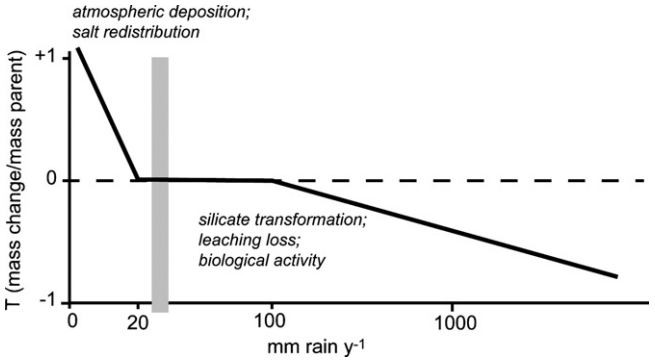

Fig. 13. Schematic of trends in total mass change with rainfall for comparably aged ($\sim 10^6$ y), temperate (MAT $\sim$ 16 °C) soils. In semi-arid to humid climates, soil formation over My timescales results in net mass loss through weathering that increases with rainfall (Brimhall et al., 1992; Capo and Chadwick, 1999; Chadwick et al., 1990; Riebe et al., 2004; Stonestrom et al., 1998). In arid to hyperarid climates, soil formation over My timescales results in accumulation of atmospheric deposition. At the hyperarid extreme, nearly all atmospheric additions are retained.

leaching, to hyperarid soils formed by ongoing addition of mass from atmospheric deposition (Fig. 13).

At Altamira and Yungay, where apparent weathering losses are minimal (Fig. 12b), the calculated total mass gain values based on immobile element (Zr) concentrations ($\overline{M} = +604 \pm 487$ and 762 ± 488 kg m^{-2}, respectively) agree well with the total measured mass of salts ($m_s = 708 \pm 106$ and 833 ± 131 kg m^{-2}, respectively; Fig. 12a). This is consistent with our assumption that immobile element concentrations in alluvium and dust have been generally similar, and indicates that our calculated mass gains reflect salt additions only. While the doubling of the soil mass and volume by solute additions alone is striking, the additional presence of substantial silicates in the deposition samples (63%) indicates that total atmospheric inputs also include substantial silicate dust. This silicate dust is likely retained unaltered in the more hyperarid soils, but is subject to in situ weathering under arid conditions at Copiapó (Fig. 12b). Quantification of these silicate dust inputs in future work may show that the total mass addition to these soils is considerably greater than the amounts calculated here.

The arid–hyperarid transition on Earth marks a shift from biotic to largely abiotic conditions (Navarro-Gonzalez et al., 2003; Warren-Rhodes et al., 2006), and accordingly we observed a pronounced decrease in soil organic C with decreasing rainfall (Fig. 12d). All life on Earth is linked with water, and a decline in biology is thus linked with a corresponding decline in all processes requiring the presence of water, including solute leaching. This work shows that with decreasing rainfall, increasingly soluble salts are retained in soils as a function of decreased leaching: total chloride and nitrate are balanced by water-soluble sodium, and are highest in the Yungay soil (230 and 17 kg m^{-2}, respectively), while the sulfate inventory at Copiapó (64 kg m^{-2}) is several times smaller than accumulations of sulfate at Altamira (457 kg m^{-2}) and Yungay (260 kg m^{-2}) (Fig. 12c). Carbonate is the exception, decreasing from Copiapó (49 kg m^{-2}) to Altamira (32 kg m^{-2}) and Yungay (23 kg m^{-2}) (Fig. 12d) as a result of sharply reduced biological activity, decreased sulfate leaching, and transient conditions of low pH (Doner and Lynn, 1989; Quinn et al., 2005). In semiarid to arid soils, carbonate retention *increases* with decreasing rainfall due to decreased leaching in generally biotic soils (Retallack, 2005). Here, the soil carbonate inventory *decreases* with decreasing rainfall, while highly bioavailable nitrate increases. These trends are the consequence of the near-absence of both biology and dissolved losses in hyperarid soils, making them fundamentally different from other soils on Earth.

These arid to hyperarid soils provide a climatic complement to the wealth of ecological and Earth system process information derived from study of semiarid to hyperhumid soils in the Hawaiian Islands (e.g., Chadwick et al., 1999), particularly with respect to the role of atmospheric inputs in soil formation (e.g., Kurtz et al., 2001). Likewise, the study of desert soils in North America and elsewhere has provided a rich and detailed perspective of soil processes under dry conditions, yet these studies have largely focused on relatively "humid" and biotic soils, in which nutrient cycling is rapid and continuous, and a large portion of atmospheric inputs is lost to leaching (Kurtz et al., 2001; Walvoord et al., 2003). This study of Atacama Desert soils captures the transition to truly water limited conditions, in which biology, silicate transformation, and leaching losses are no longer the dominant forces in pedogenesis (Fig. 13). Instead, the geochemistry of these soils reflects the profound change that occurs when atmospheric inputs and extremely limited amounts of water become the primary processes of soil formation.

4. Conclusions

With decreasing rainfall and biotic activity in northern Chile, soil formation cross a fundamental threshold in soil formation, from net long-term mass loss due to biogeochemical alteration of geologic substrate, to increasing soil volume with retention of atmospheric inputs that can exceed the mass of the silicate parent material after 10^6 y. This arid–hyperarid threshold marks the near-cessation of leaching losses, silicate transformation, and biological activity, key processes in pedogenesis almost everywhere on Earth. When long-term hyperaridity minimizes these processes, the result is soils composed primarily of atmospheric salts and dust, which physically expand the landscape as they form.

Soil geochemistry in this region is not only a unique reflection of long-term atmospheric deposition; soil depth trends and morphology also record subtle variations in climate over the past several million years. The climate history of the Atacama Desert is a function of regional

to global scale forcings fundamental to our understanding of Earth's overall climate history, and the coupled processes of landscape evolution and soil formation in this region are therefore central to that history. This work shows that a combined understanding of both landform age and the processes revealed by hyperarid soil properties provide key clues about the magnitude and duration of long-term variations in rainfall in the Atacama Desert.

The hyperarid pedogenic processes observed here provide a powerful terrestrial analog for accumulation of atmospheric dust and solutes in ancient landscapes on Mars. Martian soils contain quantities of sulfate and chloride comparable to those of hyperarid Atacama soils (Gellert et al., 2004). However, interpretation of the growing geochemical dataset for Mars is still the subject of considerable debate. Both vertical redistribution of solutes and dust deposition have been argued (Gellert et al., 2004; Clark et al., 2005; Yen et al., 2005), with critical implications for Mars climate history. Ultimately, the most hyperarid Atacama soils can help to illuminate the nature of surface processes on Mars.

Acknowledgments

Funding for this work was provided by grants to RA from NASA-Ames and the National Science Foundation. SE is grateful for a Graduate Student Research Fellowship from NASA. SSC acknowledges the National Oceanic and Atmospheric Administration for support under grant #NA16GP2360. We also thank two anonymous reviewers for key suggestions that greatly improved this paper. We thank Professor Guillermo Chong for advice and insight into the Atacama Desert and its history. We thank S. Kohl and staff at the Desert Research Institute for aerosol analysis in 2002, and P. Fine for assistance with portable aerosol sampler selection. Kim Warren-Rhodes provided critical assistance with fieldwork and nitrate analysis. We thank F. Kober for ^{21}Ne analysis. We thank M. Jimenez-Cruz for assistance with synchrotron-XRF analysis, and acknowledge the staff and support of the Advanced Light Source, Lawrence Berkeley National Laboratory. The Advanced Light Source is supported by the Director, Office of Science, Office of Basic Energy Sciences, of the U.S. Department of Energy under Contract No. DE-AC02-05CH11231.

Associate editor: Donald L. Sparks

References

Alpers, C.N., Brimhall, G.H., 1988. Middle Miocene climatic change in the Atacama desert, northern Chile: evidence from supergene mineralization at La Escondida. *Geol. Soc. Am. Bull.* **100**, 1640–1656.

Amundson, R., 2001. The carbon budget in soils. *Annu. Rev. Earth Planet. Sci.* **29**, 535–562.

Amundson, R., 2004. Soil formation. In: Drever, J.I. (Ed.), *Treatise on Geochemistry vol. 5, Surface and Ground Water Weathering and Soils*. Elsevier.

Arévalo, C., 1995. Mapa Geológico de la Hoja Copiapó (1:100,000): Región de Atacama. Servicio Nacional de Gología y Minería, documentos de Trabajo No. 8.

Aydin, A., DeGraff, J.M., 1988. Evolution of polygonal fracture patterns in lava flows. *Science* **239**, 471–476.

Bao, H., 2005. Sulfate in modern playa settings and in ash beds in hyperarid deserts: implication for the origin of 17O-anomalous sulfate in an Oligocene ash bed. *Chem. Geol.* **214**, 127–134.

Bao, H., Jenkins, K.A., Khachaturyan, M., Chong Díaz, G., 2004. Different sulfate sources and their post-depositional migration in Atacama soils. *Earth Planet. Sci. Lett.* **224**, 577–587.

Berger, I.A., Cooke, R.U., 1997. The origin and distibution of salts on alluvial fans in the Atacama Desert, northern Chile. *Earth Surf. Process. Landforms* **22**, 581–600.

Bergin, M.H., Jaffrezo, J.L., Davidson, C.I., Dibb, J.E., Pandis, S.N., Hillamo, R., Maenaut, W., Kuhns, H.D., Makela, T., 1995. The Contribution of Snow, Fog, and Dry Deposition to the Summer Flux of Anions and Cations at Summit, Greenland. *J. Geophys. Res. Atmos.* **100** (D8), 16275–16288.

Betancourt, J.L., Latorre, C., Rech, J.A., Quade, J., Rylander, K.A., 2000. A 22,000-year record of monsoonal precipitation from northern Chile's Atacama Desert. *Science* **289**, 1542–1546.

Birkeland, P., 1999. *Soils and Geomorphology*. Oxford University Press, New York, 430p.

Böhlke, J.K., Ericksen, G.E., Revesz, K., 1997. Stable isotope evidence for an atmospheric origin of desert nitrate deposits in northern Chile and southern California, USA. *Chem. Geol.* **136**, 135–152.

Brimhall, G.H., Dietrich, W.E., 1987. Constitutive mass balance relations between chemical composition, volume, density, porosity, and strain in metasomatic hydrochemical systems: results on weathering and pedogenesis. *Geochim. Cosmochim. Acta* **51**, 567–587.

Brimhall, G.H., Chadwick, O.A., Lewis, C.J., Compston, W., Williams, I.S., Danti, K.J., Dietrich, W.E., Power, M.W., Hendricks, D., Bratt, J., 1992. Deformational mass transport and invasive processes in soil evolution. *Science* **255**, 695–702.

Butler, J.N., 1982. *Carbon Dioxide Equilibria and Their Applications*. Addison-Wesley, Reading, MA.

Capo, R.C., Chadwick, O.A., 1999. Sources of strontium and calcium in desert soil and calcrete. *Earth Planet. Sci. Lett.* **170**, 61–72.

Cereceda, P., Osses, P., Larrain, H., Farías, M., Lagos, M., Pinto, R., Schemenauer, R.S., 2002. Advective, orographic and radiation fog in the Tarapacá region, Chile. *Atmos. Res.* **64**, 261–271.

Chadwick, O.A., Brimhall, G.H., Hendricks, D.M., 1990. From a black box to a gray box—a mass balance interpretation of pedogenesis. *Geomorphology* **3**, 369–390.

Chadwick, O.A., Derry, L.A., Vitousek, P.M., Huebert, B.J., Hedin, L.O., 1999. Changing sources of nutrients during four million years of ecosystem development. *Nature* **397**, 491–497.

Chadwick O.A., Goldstein R.D., 2004. Control of dilation and collapse during weathering and soil formation on Hawaiian basalts. In: *Conference on Water–Rock Interaction*.

Chatterji, S., Jeffrey, J.W., 1963. Crystal growth during hydration of $CaSO_4$–$1/2H_2O$. *Nature* **200**, 463.

Chuck, A.L., Turner, S.M., Liss, P.S., 2002. Direct evidence for a marine source of C1 and C2 alkyl nitrates. *Science* **297**, 1151–1154.

Clark, A.H., Mortimer, C., Sillitoe, R.H., Cooke, R.U., Snelling, N.J., 1967. Implications of isotopic ages of ignimbrite flows, southern Atacama Desert, Chile. *Nature* **215**, 723–1967.

Clark, A.H., Tosdal, R.M., Farrar, E., Plazolles, E., 1990. Geomorphologic environment and age of supergene enrichment of the Cuajone, Quellaveco, and Toquepala porphyry copper deposits, southeastern Peru. *Econ. Geol. Bull. Soc. Econom. Geol.* **85**, 1604–1628.

Clark, B.C., Morris, R.V., McLennan, S.M., Gellert, R., Jolliff, B., Knoll, A.H., Squyres, S.W., Lowenstein, T.K., Ming, D.W., Tosca, N.J., Yen, A., Christensen, P.R., Gorevan, S., Bruckner, J., Calvin, W.,

Deibus, G., Farrand, W., Klingelhoefer, G., Waenke, H., Zipfel, J., Bell, J.F., Grotziner, J., McSween, H.Y., Rieder, R., 2005. Chemistry and mineralogy of outcrops at Meridiani Planum. *Earth Planet. Sci. Lett.* **240**, 73–94.

Darwin, C., 1906. *The Voyage of the Beagle*. J.M. Dent, New York.

Deino, A., Potts, R., 1990. Single-crystal $^{40}Ar/^{39}Ar$ dating of the Olorgesailie Formation, Southern Kenya Rift. *J. Geophys. Res.* **95**, 8453–8470.

Doner, H.E., Lynn, W.C., 1989 Carbonate, halide, sulfate and sulfide minerals. In: Dixon, J.B., Weed, S.B. (Eds.), *Minerals in Soil Environments*. Soil Science Society of America (SSSA Book Series: No. 1), pp 279–330.

Dong, H., Rech, J.A., Jiang, H., Sun, H., Buck, B.J., 2006. Endolithc cyanobacteria in soil sulfates from hyperarid environments on Earth. Geological Society of America annual meeting, paper no. 216-3.

Dunai, T.J., Lopez, G.A.G., Juez-Larre, J., 2005. Oligocene–Miocene age of aridity in the Atacama Desert revealed by exposure dating of erosion-sensitive landforms. *Geology* **33**, 321–324.

Eckardt, F.D., Drake, N., Goudie, A.S., White, K., Viles, H., 2001. The role of playas in pedogenic gypsum crust formation in the Central Namib Desert: a theoretical model. *Earth Surf. Process. Landforms* **26**, 1177–1193.

Eckardt, F.D., Spiro, B., 1999. The origin of sulphur in gypsum and dissolved sulphate in the Central Namib Desert, Namibia. *Sediment. Geol.* **123** (3–4), 255–273.

Ericksen, G.E., 1981. *Geology and origin of the Chilean nitrate deposits*. Geological Society Professional Paper 1188. Unites States Government Printing Office, Washington.

Ewing, S.A., Michalski, G., Wu, J., Amundson, R., Thiemens, M., McKay, C.P., 2005. Limited biology preserves atmospheric N in Atacama Desert soils. In: *Abstracts of Papers of the Americal Chemical Society* 229, U889-U889 046-GEOC Part 1, March 13, 2005 (oral presentation).

Ewing, S.A., Navarro-González, R., Amundson, R.G., Wu, J., McKay, C.P., 2004. A soil carbon cycle without life? The content and residence times of organic carbon in the Atacama Desert of Chile. *Int. J. Astrobiol.* Supplement, 71.

Galloway, J.N., Dentener, F.J., Capone, D.G., Boyer, E.W., Howarth, R.W., Seitzinger, S.P., Asner, G.P., Cleveland, C.C., Green, P.A., Holland, E.A., Karl, D.M., Michaels, A.F., Porter, J.H., Townsend, A.R., Vorosmarty, C.J., 2004. Nitrogen cycles: past, present, and future. *Biogeochemistry* **70**, 153–226.

Gellert, R., Rieder, R., Anderson, R.C. Brückner, J., Clark, B.C., et al., 2004. Chemistry of rocks and soils in Gusev Crater from the alpha particle X-ray spectrometer. *Science* **305**, 829–832.

Godoy, E., Lara, L., 1998. *Hoja Quebrado Salitrosa, Región de Atacama*. Servicio Nacional de Geología y Minería, Mapas Geológicos No. 4 (1:100,000).

Goehring, L., Morris, S.W., 2005. Order and disorder in columnar joints. *Europhys. Lett.* **69**, 739–745.

Harris, D.C., 1995. *Quantitative Chemical Analysis*, 4th ed. W.H. Freeman and Company, New York, 122 pp.

Hartley, A.J., Chong, G., 2002. Late Pliocene age for the Atacama Desert: implications for the desertification of western South America. *Geology* **31**, 4346.

Hartley, A.J., Chong, G., Houston, J., Mather, A.E., 2005. 150 million years of climatic stability: evidence from the Atacama Desert, northern Chile. *J. Geol. Soc.* **162**, 421–424.

Hartley, A.J., Rice, C.M., 2005. Controls on supergene enrichment of porphyry copper deposits in the central Andes: a review and discussion. *Mineral. Deposita* **40**, 515–525.

Holland, E.A., Dentener, F.J., Braswell, B.H., Sulzman, J.M., 1999. Contemporary and pre-industrial global reactive nitrogen budgets. *Biogeochemistry* **46**, 7–43.

Houston, J., Hartley, A.J., 2003. The central Andean west-slope rainshadow and its potential contribution to the origin of hyperaridity in the Atacama Desert. *Int. J. Climatol.* **23**, 1453–1464.

Jury, W.A., Gardner, W.R., Gardner, W.H., 1991. *Soil Physics*, 5th ed. John Wiley, New York.

Kessler, M.A., Werner, B.T., 2003. Self-organization of sorted patterned ground. *Science* **299**, 380–383.

Koch, D., Jacob, D., Tegen, I., Rind, D., Chin, M., 1999. Tropospheric sulfur simulation and sulfate direct radiative forcing in the Goddard Institute for Space Studies general circulation model. *J. Geophys. Res. Atmos.* **104** (D19), 23799–23822.

Kohl, C.P., Nishiizumi, K., 1992. Chemical isolation of quartz for measurement of in situ produced cosmogenic nuclides. *Geochim. Cosmochim. Acta* **56**, 3583–3587.

Kurtz, A.C., Derry, L.A., Chadwick, O.A., 2001. Accretion of Asian dust to Hawaiian soils: isotopic elemental and mineral mass balances. *Geochim Cosmochim Acta* **65**, 1971–1983.

Kurtz, A.C., Derry, L.A., Chadwick, O.A., Alfano, M.J., 2000. Refractory element mobility in volcanic soils. *Geology* **28**, 683–686.

Lal, D., 1991. Cosmic ray labeling of erosion surfaces: in situ nuclide production rates and erosion models. *Earth Planet. Sci. Lett.* **104**, 421–439.

Lamy, F., Klump, J., Hebbeln, D., Wefer, G., 2000. Late Quaternary climate change in northern Chile. *Terra Nova* **12**, 8–13.

Lara, L., Godoy, E. (1998) *Hojas Chañaral y Diego de Almagro, Región de Atacama*. Servicio Nacional de Geología y Minería, Mapas Geológicos Nos. 5–6 (1:100,000).

Larrain, H., Velásquez, F., Cereceda, P., Espejo, R., Pinto, R., Osses, P., Schemenauer, R.S., 2002. Fog measurements at the site "falda Verde" north of Chañaral compared with other fog stations of Chile. *Atmos. Res.* **64**, 273–284.

Latorre, C., Betancourt, J.L., Rylander, K.A., Quade, J., 2002. Vegetation invasions into absolute desert: a 45,000 yr rodent midden record from the Calama-Salar de Atacama basins, northern Chile (lat 22°–24 degrS). *Geol. Soc. Am. Bull.* **114**, 349–366.

Latorre, C., Betancourt, J.L., Rylander, K.A., Quade, J., Matthei, O., 2003. A vegetation history from the arid prepuna of northern Chile (22–23 degrS) over the last 13,500 years. *Palaeogeogr., Palaeoclimatol., Palaeoecol.* **194**, 223–246.

Marín, V.H., Olivares, G.R., 1999. Estacionalidad de la productividad primaria en Bahía Mejillones del Sur (Chile): una aproximación proceso-funcional. *Rev. Chilena Historia Nat.* **72**, 629–641.

Marinovic, N., Smoje, I., Maksaev, V., Hervé, M., Mpodozis, C. (1992) Hoja Aguas Blancas, Región de Antofagasta. Servicio Nacional de Geología y Minería, Carta Geológica de Chile, No. 70.

Mather, T.A., Allen, A.G., Davison, B.M., Pyle, D.M., Oppenheimer, C., McGonigle, A.J.S., 2004a. Earth Planet. *Sci. Lett.* **218**, 17–30.

Mather, T.A., Tsanev, V.I., Pyle, D.M., McGonigle, A.J.S., Oppenheimer, C., Allen, A.G. 2004b. Characterization and evolution of tropospheric plumes from Lascar and Villarrica volcanoes, Chile. J. Geophys. Res. Atmos. 109, Art. No. D21303 Nov. 4, 2004.

Matthews, S.J., Gardweg, M.C., Sparks, R.S.J., 1997. The 1984 to 1996 cyclic activity of Lascar Volcano, northern Chile: cyles of dome growth, dome subsidence, degassing, and explosive eruptions. *Bull. Volcanol.* **59**, 72–82.

McFadden, L.D., Wells, S.G., Jercinovich, M.J., 1987. Influences of eolian and pedogenic proceses on the origen and evolution of desert pavements. *Geology* **15**, 504–508.

McKay, C.P., Friedmann, I., Gómez-Silva, B., Cáceres-Villanueva, L., Anderson, D.T., Landheim, R., 2003. Temperature and moisture conditions for life in the extreme arid region of the Atacama Desert: four years of observation including the El Niño of 1997-1998. *Astrobiology* **3**, 393–406.

Michalski, G., Böhlke, J.K., Thiemens, M., 2004. Long term atmospheric deposition as the source of nitrate and other salts in the Atacama Desert, Chile: new evidence from mass-independent oxygen isotopic compositions. *Geochim. Cosmochim. Acta.* **68**, 4023–4028.

Mikhailov, I.S., 2000. Exogenesis and soil formation in the Atacama region. *Eurasian Soil Sci.* **33**, 1255–1262.

Minagawa, M., Winter, D.A., Kaplan, I.R., 1984. Comparison of Kjeldahl and combustion methods for measurement of nitrogen isotope ratios in organic matter. *Anal. Chem.* **56**, 1859–1861.

Mintz, Y., Walker, G.K., 1992. Global fields of soil moisture and land surface evapotranspiration derived from observed precipitation and surface air temperature. *J. Appl. Meteorol.* **32**, 1305–1334.

Moore, R.M., Blough, N.V., 2002, A marine source of methyl nitrate. *Geophys. Res. Lett.* **29**. doi:10.1029/2002GL014989.

Moore, J.K., Doney, S.C., Glover, D.M., Fung, I.Y., 2002. Iron cycling and nutrient limitation patterns in surface waters of the world ocean. *Deep-Sea Res. Part II—Topical Studies Oceanog.* **49**, 463–507.

Mortimer, C., 1973. The Cenozoic history of the southern Atacama Desert, Chile. *J. Geol. Soc. Lond.* **129**, 505–526.

Mortimer, C., 1980. Drainage evolution in the Atacama desert of northern Chile. *Revista Geológica de Chile* **11**, 3–28.

Naranjo, J.A., Puig, A. (1984) Taltal y Chañaral. Servicio Nacional de Geología y Minería, Carta Geolóica de Chile, Nos. 62-63 (escala 1:250,000).

Navarro-Gonzalez, R., Rainey, F.A., Molina, P., Bagaley, D.R., Hollen, B.J., de la Rosa, J., Small, A.M., Quinn, R.C., Grunthaner, F.J., Caceres, L., Gomez-Silva, B., McKay, C.P., 2003. Mars-like soils in the Atacama Desert, Chile, and the dry limit of microbial life. *Science* **302** (5647), 1018–1021.

Nishiizumi, K., Kohl, C.P., Arnold, J.R., Klein, J., Fink, D., Middleton, R., 1991. Cosmic ray produced ^{10}Be and ^{26}Al in Antarctic rocks: exposure and erosion history. *Earth Planet. Sci. Lett.* **104**, 440–454.

Nishiizumi, K., Caffee, M.W., Finkel, R.C., Brimhall, G., Mote, G., 2005. Remnants of a fossil alluvial fan landscape of Miocene age in the Atacama Desert of northern chile using cosmogenic nuclide exposure age dating. *Earth Planet. Sci. Lett.* **237**, 499–507.

Owen, J., Nishiizumi, K., Sharp, W., Sutter, B., Ewing, S., Amundson, R., 2003. Investigations into the Numerical Ages of post-Miocene Fluvial Landforms in the Atacama Desert, Chile. *Eos Trans.* AGU, **84**, Fall Meet. Suppl., Abstract T31C-0857.

Perry, K.D., Cliff, S.S., Jimenez-Cruz, M.P., 2004. Evidence for hygroscopic mineral dust particles from the Intercontinental Transport and Chemical Transformation Experiment, *J. Geophys. Res.* **109**, D23S28. doi:10.1029/2004JD004979.

Pueyo, J.J., Chong, G., Vega, M., 1998. Mineralogy and parental brine evolution in the Pedro de Valdivia nitrate deposit, Antofagasta, Chile. *Revista Geologica de Chile* **25**, 3–15.

Quade, J., Chivas, A.R., McCulloch, M.T., 1995. Strontium and carbon isotope tracers and the origins of soil carbonate in South Australia and Victoria. *Palaeogeogr, Palaeoclimatol., Palaelecol.* **113**, 103–117.

Quinn, R.C., Zent, A.P., Grunthaner, F.J., Ehrenfreund, P., Taylor, C.L., Garry, J.R.C., 2005. Detection and characterization of oxidizing acids in the Atacama Desert using the Mars Oxidation Instrument. *Planet. Space Sci.* **53** (13), 1376–1388.

Ravelo, A.C., Andreasen, D.H., Lyle, M., Lyle, A.O., Wara, M.W., 2004. Regional climate shifts caused by gradual global cooling in the Pliocene epoch. *Nature* **429**, 263–267.

Rech, J.A., Quade, J., Hart, W.S., 2003. Isotopic evidence for the source of Ca and S in soil gypsum, anhydrite and calcite in the Atacama Desert, Chile. *Geochim. Cosmochim. Acta* **67**, 575–586.

Reheis, M.C., Kihl, R., 1995. Dust deposition in southern Nevada and California, 1984-1989 – relations to climate, source area, and source lithology. *J. Geophys. Res. Atmosph.* **100** (D5), 8893–8918.

Riebe, C.S., Kirchner, J.W., Finkel, R.C., 2003. Long-term chemical weathering rates and physical erosion from cosmogenic nuclides and geochemical mass balance. *Geochim. Cosmochim. Acta* **67** (22), 4411–4427.

Riebe, C.S., Kirchner, J.W., Finkel, R.C., 2004. Erosional and climatic effects on long-term chemical weathering rates in granitic landscapes spanning diverse climate regimes. *Earth Planet. Sci. Lett.* **224**, 547–562.

Riebe, C.S., Kirchner, J.W., Granger, D.E., Finkel, R.C., 2001. Strong tectonic and weak climatic control of long-term chemical weathering rates. *Geology* **29** (6), 51–514.

Renne, P.R., Swisher III, C., Deino, A.L., Karner, D.B., Owens, T., DePaolo, D.J., 1998. Intercalibration of standards, absolute ages and uncertainties in ^{40}Ar/^{39}Ar dating. *Chem. Geol.* **145** (1–2), 117–152.

Retallack, G.J., 2005. Pedogenic carbonate proxies for amount and seasonality of precipitation in paleosols. *Geology* **33** (4), 333–336.

Rojas, C.M., Figueroa, L., Hanssens, K.H., Van Espen, P.E., Adams, F.C., Van Greiken, R.E., 1990. The elemental composition of airborne particulate matter in the Atacama Desert, Chile. *Sci. Tot. Env.* **91**, 251–267.

Schaeffer, S.M., Evans, R.D., 2005. Pulse additions of soil carbon and nitrogen affect soil nitrogen dynamics in an arid Colorado Plateau shrubland. *Oecologia* **145**, 425–433.

Schemenauer, R.S., Cereceda, P., 1992. the quality of fog water collected for domestic and agricultural use in Chile. *J. Appl. Meteorol.* **31**, 275–290.

Searl, A., Rankin, S., 1993. A preliminary petrographic study of the Chilean nitrates. *Geol. Mag.* **130**, 319–333.

Seinfeld, J.H., Pandis, S.N., 1998. *Atmospheric Chemistry and Physics: from Air Pollution to Climate Change*. John Wiley.

Soil Survey Staff . 1999. Keys to Soil Taxonomy. Pocahontas Press Inc, Blacksburg, VA.

Spiro, B., Eckardt, F.D., 1999. The origin of sulphur in gypsum and dissolved sulphate in the Central Namib Desert, Namibia. *Sediment. Geol.* **123**, 255–273.

Stonestrom, D.A., White, A.F., Akstin, K.C., 1998. Determining rates of chemical weathering in soils—solute tanport versus profile evolution. *J. Hydrol.* **209**, 331–345.

Thiemens, M.H., Savarino, J., Farquhar, J., Bao, H.M., 2001. Mass-independent isotopic compositions in terrestrial and extraterrestrial solids and their applications. *Accounts Chem. Res.* **34**, 645–652.

Torres, A.L., Thompson, A.M., 1993. Nitric oxide in the equatorial Pacific boundary layer: SAGA 3 measurements. *J. Geophys. Res. Atmos.* **98**, 16949–16954.

Toramaru, A., Matsumoto, T., 2004. Columnar joint morphology and cooling rate: a starch–water mixture experiment. *J. Geophys. Res.* **109**, 1–10.

Tyler, S.W., Chapman, J.B., Conrad, S.H., Hammermeister, D.P., Blout, D.O., Ginanni, J.M., 1996. Soil–water flux in the southern Great Bain, United States: temporal and spatial variations over the last 120,000 years. *Water Resources Res.* **32**, 1481–1499.

UNEP/GRID (United Nations Environment Program/Global Resource Information Database) (1991) Global digital data sets for land degradation studies: a GIS approach. Prepared by U. Deichmann and L. Eklundh. GRID Case Study Series No. 4. UNEP/GEMS and GRID. Nairobi, Kenya.

Vuille, M., Keimig, F., 2004. Interannual variability of summertime convective cloudiness and precipitation in the central Andes derived from ISCCP-B3 data. *J. Climate* **17**, 3334–3348.

Walvoord, M.A., Phillips, F.M., Stonestrom, D.A., Evans, R.D., Hartsough, P.C., Newman, B.D., Striegl, R.G., 2003. A reservoir of nitrate beneath desert soils. *Science* **302**, 1021–1024 (and supporting online material).

Warren-Rhodes, K., Rhodes, K.L., Pointing, S.B., Ewing, S., Lacap, D.C., Gómez-Silva, B., Amundson, R., Friedmann, E.I., McKay, C.P., 2006. The influence of water availability on cyanobacterial community ecology and the dry limit to photosynthetic life in the Atacama Desert, *Chile. Microbial Ecol.*

Wara, M.W., Ravelo, A.C., Delaney, M.L., 2005. Permanent El Niño like conditions during the Pliocene warm period. *Science* **309**, 758–761.

Whittig, L.D., Allardice, W.R., 1986. X-ray diffraction techniques. p. 331-362. In ed. A. Klute. Methods of Soil analysis part 1: Physical and mineralogical methods. 2nd ed. ASA, SSSA, Madison, WI.

Wierzchos, J., Ascaso, C., McKay, C.P., 2006. Endolithic cyanobacteria in halite rocks from the hyperarid core of the Atacama Desert. *Astrobiology* **6** (3), 415–422.

Yen, A., Gellert, R., Schroder, C., Morris, R.V., Bell III, J.F., Knudson, A.T., Clark, B.C., Ming, D.W., Crisp, J.A., Arvidson, R.E., Blaney, D., Bruckner, J., Christensen, P.R., DesMarais,

D.J., de Souza, P.A. Jr., Economou, T.E., Ghosh, A., Hahn, B.C., Herkenhoff, K.E., Haskin, L.A., Hurowitz, J.A., Joliff, B.L., Johnson, J.R., Klingelhofer, G., Madsen, M.B., McLennan, S.M., McSween, H.Y., Richter, L., Rieder, R., Rodionov, D., Soderblom, L., Squyres, S.W., Tosca, N.J., Wang, A., Wyatt, M., Zipfel, J., 2003. An integrated view of the chemistry and mineralogy of martian soils. *Nature* **436**, 49–54 (doi:10.1038/nature03637).

Yvon, S.A., Saltzman, E.S., 1996. Atmospheric sulfur cycling in the tropical Pacific marine boundary layer (12 degrees S, 135 degrees W): a comparison of field data and model results. 2. Sulfur dioxide. *J. Geophys. Res. Atmos.* **101**, 6911–6918.

Zhang, Q., Anastasio, C., 2003. Conversion of fogwater and aerosol organic nitrogen to ammonium, nitrate, and NOx during exposure to simulated sunlight and ozone. *Environ. Sci. Technol.* **37** (16), 3522–3530.